ENGINEERING RESEARCH INSTITUTE
UNIVERSITY OF MICHIGAN
ANN ARBOR

REVERSIBLE SUSCEPTIBILITY IN FERRIMAGNETIC MATERIALS

Technical Report No. 24
Electronic Defense Group
Department of Electrical Engineering

By: D. M. Grimes
D. W. Martin

Approved by: H. W. Welch, Jr.

Project 1970

TASK ORDER NO. EDG-6
CONTRACT NO. DA-36-039 sc-15358
SIGNAL CORPS, DEPARTMENT OF THE ARMY
DEPARTMENT OF ARMY PROJECT NO. 3-99-04-042
SIGNAL CORPS PROJECT NO. 29-194B-0

May, 1954

TABLE OF CONTENTS

LIST OF ILLUSTRATIONS

ABSTRACT

Expressions for the reversible susceptibility both normal to and parallel with an applied biasing field are given. The theoretical basis for these expressions is considered. Experimental data for three different ferrite specimens are given. Qualitative deviations from the reversible equations are considered assuming domain wall motion to be retarded by large potential holes. The averaging effect of toroidal geometry is considered in some detail.

REVERSIBLE SUSCEPTIBILITY IN FERRIMAGNETIC MATERIAL

1. INTRODUCTION AND DEFINITIONS

The parallel reversible susceptibility in ferromagnetic material has been the subject of several authors since it was discussed by R. Gans[1] in 1911. A recent paper which includes a review of the experimental status is that of Tebble and Corner[2].

The reversible susceptibility χ_{rp} is customarily defined as:

$$\chi_{rp} = \lim_{\Delta H \to 0} \frac{\Delta M}{\Delta H} \tag{1}$$

where ΔH has a sense opposite to that of the change in H which brought the specimen to the point (M,H). The differential susceptibility, χ_d, differs from the reversible susceptibility in that ΔH is taken in the same sense as the change in H which brought the material to the point (M,H). χ_d is, in general, larger than χ_{rp}. It is assumed that if a vanishingly small ac field is applied such that ΔH is alternately parallel and antiparallel with the aforedescribed direction of H the resulting susceptibility will be the parallel reversible susceptibility.

The transverse reversible susceptibility, χ_{rt}, is hereby defined as:

$$\chi_{rt} = \lim_{\Delta H \to 0} \left(\frac{\Delta M}{\Delta H} \right) \tag{2}$$

where ΔH is perpendicular to the direction in which H was changed to bring the specimen to the point (M,H) and thus also perpendicular to the direction ΔH used to measure the parallel reversible susceptibility.

The initial susceptibility χ_o is defined as:

$$\chi_o = \lim_{M \to 0} \chi_r \tag{3}$$

2. THEORETICAL DEVELOPMENT

2.1 The Initial Susceptibility

Since the magnetic moment per unit volume is given by

$$M = \sum_{\text{all atoms}} \mu_\beta \, g \, \frac{\vec{S} \cdot \vec{H}}{H} \, , \tag{4}*$$

evidently changes in M occur by means of changes in the net spin $\vec{S}$ aligned in the direction of the field. Three possible mechanisms of change are illustrated in Figs. 1a, 1b, and 1c.

In Fig. 1a, before the application of an external field a domain wall is located at the position x. When the field is applied the wall moves to a position $x + \Delta x$. All atoms between x and $x + \Delta x$ must undergo a 180^o reversal in direction of their magnetic moment. In Fig. 1b the solid arrow may rotate to the position shown by the dashed arrow. For the same ΔM as in 1a, a much larger number of atoms must rotate through a small angle θ. Fig. 1c shows still another possibility.

* μ_β is the Bohr magneton, g is the Lande g factor, $\vec{S}$ is the net ionic spin in units of $\hbar$, $\vec{H}$ is the applied magnetic field.

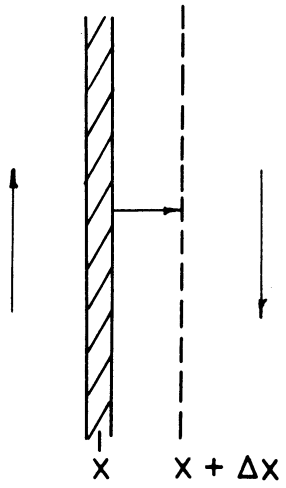

FIG Ia

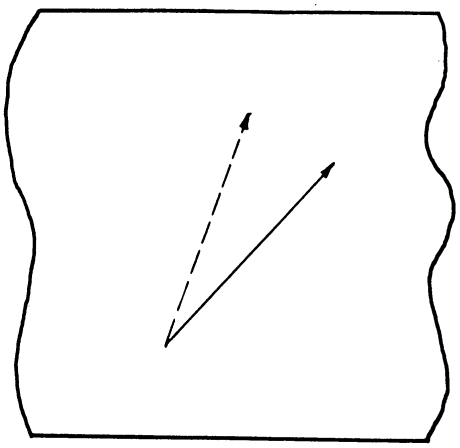

FIG Ib

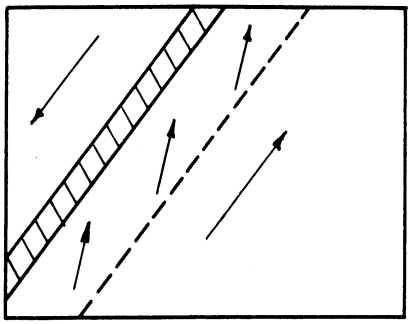

FIG Ic

POSSIBLE MECHANISMS OF MAGNETIZATION CHANGES

The question of whether the low frequency initial permeability in ferrites arises from wall movement (Fig. 1a) or rotation (Figs. 1b, 1c) was rather convincingly answered by Rado[3], et al. They measured the spectrum of permeability versus frequency for a ferrite, then ground it to single-domain-size particles and remeasured. They concluded that the low frequency initial permeability is primarily due to wall movement as shown in Fig. 1a.

The variation with the position of a domain wall in the energy of a ferromagnetic body appears similar to Fig. 2. We now wish to determine the relationship between the shape of the potential curve and the initial susceptibility.

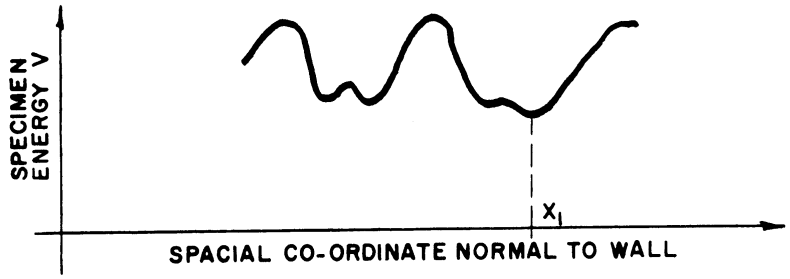

FIG 2. SPECIMEN ENERGY VS WALL SPACIAL CO-ORDINATE

In the absence of an external field, the wall will come to rest at a minimum energy position such as x_1. If the energy function is assumed to be a continuous function of position it can be expanded into a Taylor series:

$$V(x) = V(x_1) + \frac{1}{2\rho_r}(x-x_1)^2 \tag{5}$$

where ρ_r is the radius of curvature of V(x) at the point $x = x_1$. When a reversible field is applied, the potential $V^*(x)$ is given by:

$$V^*(x) = V(x) - \gamma M_s x \, dH \tag{6}$$

for a wall of unit area. γ is a constant depending upon the type of wall considered.

Combine Eqs. 5 and 6 and differentiate to obtain:

$$\frac{d\,V^*(x)}{dx} = \frac{1}{\rho_r}\,(x-x_1) - \gamma\, M_s\, dH \tag{7}$$

The minimum energy condition is then:

$$x - x_1 = \rho_r\, \gamma\, M_s\, dH \tag{8}$$

The magnetization and susceptibility associated with this initial reversible field for a wall of unit area is then:

$$dM_r = \gamma\, M_s\,(x-x_1) = \rho_r\, \gamma^2\, M_s^2\, dH$$

$$\chi_o = \rho_r\, \gamma^2\, M_s^2 \tag{9}$$

The problem of evaluating χ_o thus becomes one of determining ρ_r and the wall area located at each potential minimum.

Becker and Doring[4] assumed a system of cubical domains, 90^o walls, and a sinusoidal variation in internal stresses and obtained:

$$\chi_o = \frac{4M_s^2}{3\pi\,\lambda_s\,\sigma_i} \tag{10}$$

where λ_s is the saturation magnetostriction and σ_i is some average value of internal stresses. This is found to agree quite well with experiment both in parameter dependence and in magnitude. However, this does not substantiate an assumption that χ_o must have its origin at least predominately in wall movement for Kersten[5] obtained a result:

$$\chi_o = \frac{2M_s^2}{9\ \lambda_s\ \sigma_i} \tag{11}$$

assuming only rotational processes.

2.2 The Parallel Reversible Susceptibility

Gans first suggested the parametric equations

$$\frac{M}{M_s} = f(\eta) \quad ; \quad \frac{\chi_{rp}}{\chi_o} = 3f'(\eta) \tag{12}$$

where $f(\eta) = L(\eta)$, the Langevin function:

$$L(\eta) = \left(\text{ctnh}\ \eta - \frac{1}{\eta}\right) \tag{13}$$

The prime indicates $\frac{d}{d\eta}$.

It was found that this equation fit quite well the data for iron and nickel. This was first put on a semitheoretical basis by Brown[6] in 1938. To do this Brown assumed ferromagnetic material to consist of N domains per unit volume all of fixed and equal volume. These domains were considered to be subjected to random but fixed forces in such a manner that the ordinary techniques of statistical mechanics could be applied.

His development of Eq. 12 is given in the appendix. He later[7] attempted to derive these equations with a model allowing variation in domain size. However a large number of assumptions were necessary. Some are so stringent as to question whether the work is really an extension of his original papers.

2.3 The Transverse Reversible Susceptibility

If the parallel reversible susceptibility is given by Eq. 12 where $f(\eta)$ is any arbitrary continuous function of η, χ_{rt}/χ_o can be developed as follows[8]:

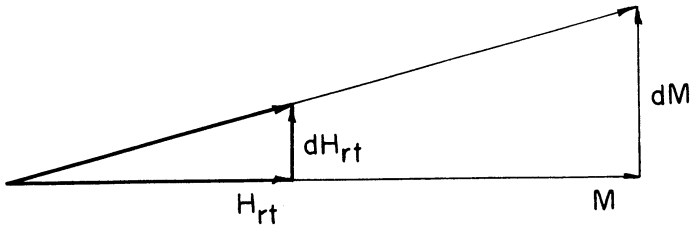

FIG 3. RELATIONSHIP FOR DETERMINING TRANSVERSE REVERSIBLE SUSCEPTIBILITY

In a multicrystalline specimen when H_r is rotated through a small angle, $(\vec{M}+d\vec{M})$ remains parallel to $\vec{H}_r + d\vec{H}_{rt}$. Thus, see Fig. 3, ($H_r$ is defined in the appendix).

$$\chi_{rt} = \frac{dM}{dH_{rt}} = \frac{M}{H_r} \tag{14}$$

Now

$$\frac{1}{\chi_{rp}} = \frac{dH_r}{dM} = \frac{d}{dM}\left(\frac{M}{\chi_{rt}}\right)$$

where the first equality is the definition of χ_{rp}, and the second follows from Eq. 14. Substituting for χ_{rp}, M, from Eq. 12, and using $dM = M_s f'(\eta)\, d\eta$,

$$\frac{1}{3\chi_o} = \frac{d}{d\eta}\left(\frac{f(\eta)}{\chi_{rt}}\right)$$

or, upon integrating

$$\frac{\chi_{rt}}{\chi_o} = 3\,\frac{f(\eta)}{\eta} \tag{15}$$

since $\chi_{rt} = \chi_{rp} = \chi_o$ when M = 0.

Brown obtains Eq. 12, from which Eq. 15 follows, for spherical and cubic symmetries. The form $F(\eta)$ varies with the exact anisotropy. Table I shows the result for two such assumptions (see appendix for derivation).

TABLE I

$f(\eta)$ FOR ISOTROPIC AND $\left[111\right]$ ORIENTED MATERIAL

Anisotropy	$f(\eta)$
isotropic	$L(\eta) = \operatorname{ctnh}\,\eta - \frac{1}{\eta}$
$\left[111\right]$	$E(\eta) = \frac{3\sqrt{3}}{\eta^2}\int_0^{\eta/\sqrt{3}} \mu \tanh \mu d\mu$

The functions $L(\eta)$ and $E(\eta)$, for small values of η, can be expanded as follows:

$$L(\eta) = \frac{\eta}{3} - \frac{\eta^3}{45} + \frac{2\eta^5}{945} - \frac{1}{4725}\,\eta^7 + \cdots\cdots$$

$$E(\eta) = \frac{\eta}{3} - \frac{\eta^3}{45} + \frac{2\eta^5}{945} - \frac{17}{76{,}545}\,\eta^7 + \cdots\cdots \tag{16}$$

These expressions are identical up to η^7. Fig. 4 shows two plots of the parametric Eq. 12 where in the upper curve $f(\eta) = L(\eta)$, and in the lower $f(\eta) = E(\eta)$. Fig. 5 shows Eq. 15, once again in the upper curve $f(\eta) = L(\eta)$, in

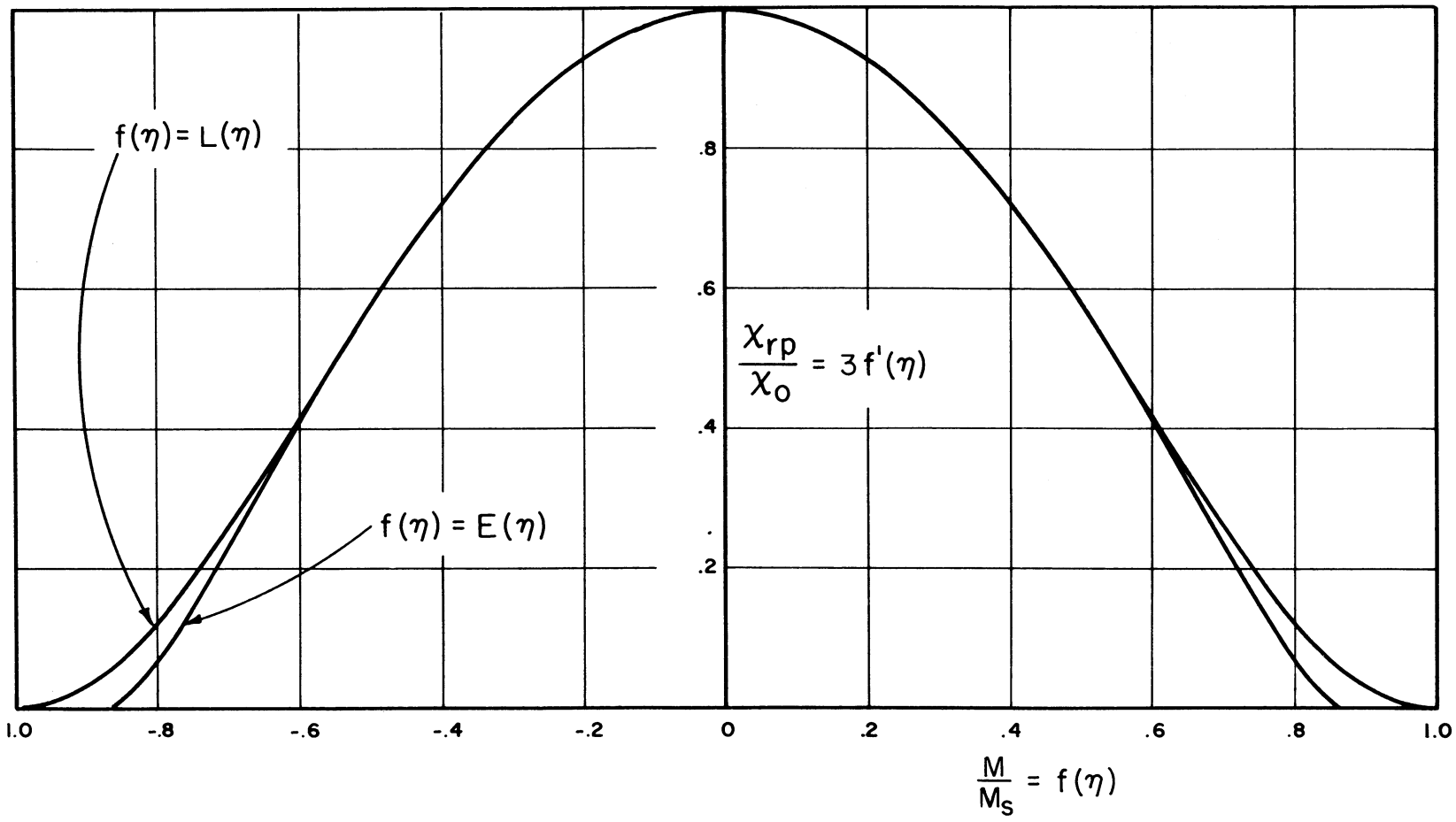

FIG 4

THEORETICAL PARALLEL REVERSIBLE SUSCEPTIBILITY VS MAGNETIZATION

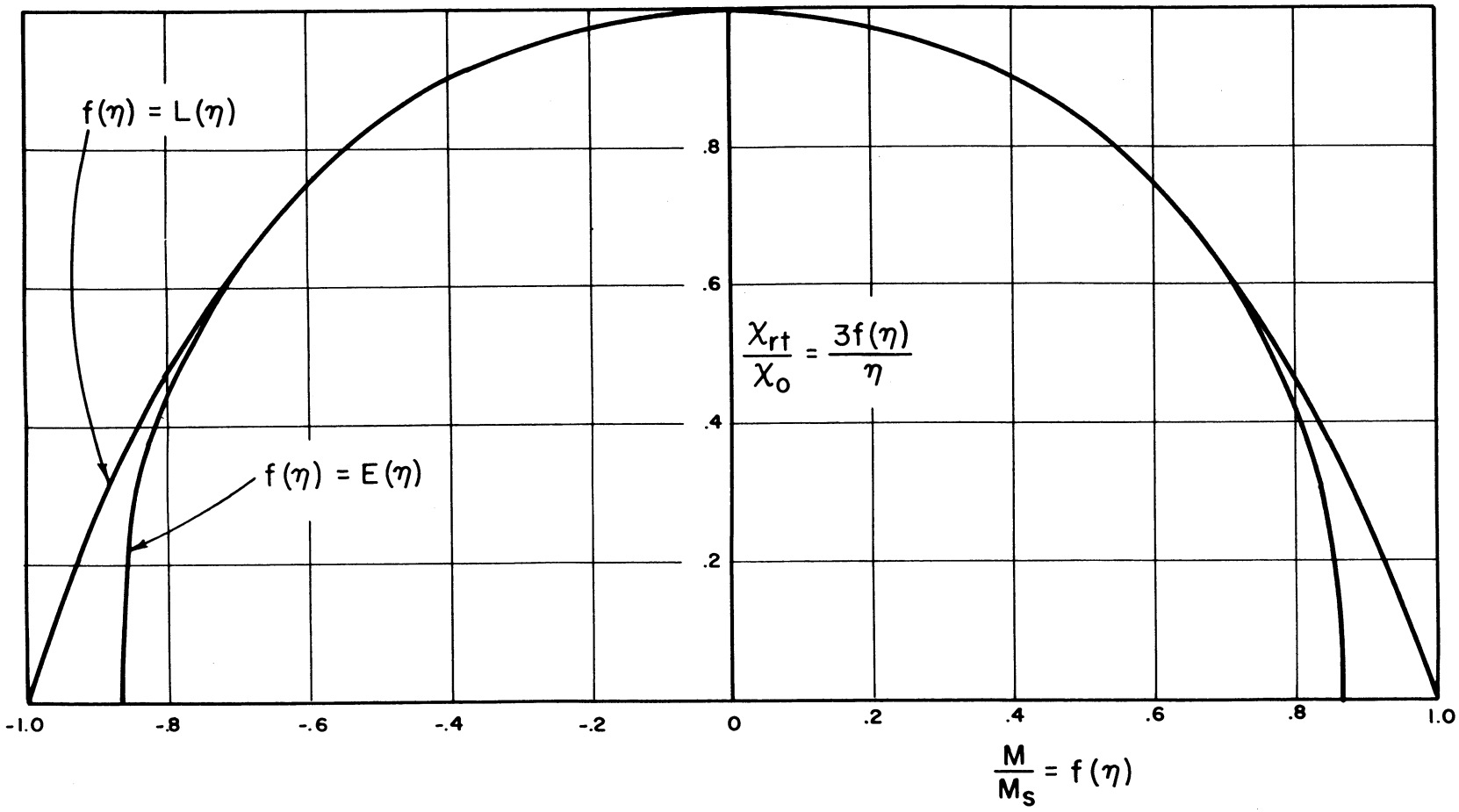

FIG 5

THEORETICAL TRANSVERSE REVERSIBLE SUSCEPTIBILITY VS MAGNETIZATION

TABLE II

M/M_s and χ_r/χ_o vs η for $f(\eta) = L(\eta)$ and $f(\eta) = E(\eta)$

η	$L(\eta)$	$3L'(\eta)$	$3\frac{L(\eta)}{\eta}$	$E(\eta)$	$3E'(\eta)$	$3\frac{E(\eta)}{\eta}$
0	0	1.000	1.000	0	1.000	1.000
.450	.148	.960	.987	.148	.960	.987
.650	.211	.920	.974	.211	.920	.974
.820	.262	.878	.959	.262	.878	.959
.960	.302	.840	.944	.302	.840	.944
1.09	.338	.801	.930	.338	.801	.930
1.22	.371	.761	.912	.371	.761	.912
1.35	.403	.719	.896	.403	.719	.896
1.47	.431	.680	.880	.431	.680	.880
1.60	.460	.640	.863	.460	.640	.863
1.73	.487	.600	.845	.487	.600	.845
1.86	.512	.561	.826	.511	.537	.824
2.01	.539	.519	.804	.538	.516	.803
2.15	.562	.481	.784	.560	.480	.781
2.31	.586	.441	.761	.585	.435	.760
2.49	.612	.400	.737	.610	.390	.735
2.68	.636	.360	.712	.634	.354	.710
2.90	.661	.329	.684	.658	.309	.681
3.15	.686	.280	.653	.682	.267	.650
3.44	.711	.240	.620	.706	.225	.616
3.82	.739	.200	.580	.731	.177	.574
4.32	.769	.160	.534	.757	.135	.526
4.98	.799	.120	.481	.782	.096	.471
5.35	.813	.105	.456	.793	.078	.445
6.10	.836	.081	.411	.809	.054	.398
7.10	.859	.059	.363	.824	.036	.348
8.10	.877	.046	.325	.833	.024	.309
9.20	.891	.035	.291	.841	.015	.274
11.00	.909	.025	.248	.848	.009	.231
13.00	.923	.018	.213	.853	.006	.197
15.00	.933	.013	.187	.857	.003	.171
20.00	.950	.007	.143	.861	.001	.129
30.00	.967	.003	.097	.864	.000	.086
75.00	.987	.001	.040	.866	.000	.035
∞	1.000	0	0	.867	0	0

the lower $f(\eta) = E(\eta)$. It is evident that both equations give identical results for the two functions at low values of magnetization.

Since $E(\eta)$ is obtained for the function $f(\eta)$ in Eqs. 12 and 15 under the assumption that the magnetization vectors can lie only in $[111]$ directions, we expect the true behaviour to approximate this case only at low fields. At higher fields domains will begin to leave $[111]$ directions so as to more nearly align with the field, and we expect the behaviour to approach that of the isotropic case. Therefore, since there is little difference between the two cases at low fields where the anisotropy is important, we expect that $f(\eta) = L(\eta)$ should be a good approximation throughout. Numerical values are given in Table II.

3. EXPERIMENTAL METHOD

3.1 Specimen Shape

In their commonest applications ferrites are generally used in the form of toroidal cores. The advantage of this shape is that closed flux paths around the ring eliminate surface poles and macroscopic demagnetizing fields. However the magnetic properties of such a core still contain certain shape-dependent factors superimposed upon the properties of the core material itself, for which it is not always possible to correct in an unambiguous way. For this reason most studies in which the properties of materials are to be measured have used other special shapes adapted to the particular experiment. For instance the parallel susceptibility is often measured on very long, thin, cylindrical specimens.

The shape best suited to one particular measurement may be highly impractical for another, as is the case for the "parallel" and "transverse" reversible susceptibilities. Yet it is desirable that both these measurements be

done on the same specimen if a comparison is to be significant, because it is very difficult to obtain reproducibility with ferrites between even supposedly identical specimens. Specimens of different shapes, even if made from the same batch and treated identically as far as possible, might have quite different properties.

The toroidal shape eliminates the demagnetizing effects for fields directed around the ring, while at the same time the lateral extent of the specimen is confined so that uniform perpendicular fields may be more readily applied. For this reason we elected to perform all of the present measurements on toroidal cores. The special difficulties which the shape introduces are taken up as they arise in the following discussion.

3.2 General Procedures

The specimens are cycled manually around their major hysteresis loops by a battery-powered dc field, hereinafter called the "bias" field. Magnetization as a function of this field is deduced from flux changes measured with a General Electric fluxmeter. The whole B-H loop is read point by point by increasing the bias field quickly from zero to the desired H, reading the flux changes, then continuing up to saturation and on around the major loop back to zero. This entire cycle is repeated for each point, so that cumulative errors in the fluxmeter readings are avoided. An array of fixed resistors and copper knife switches is used to control the bias field in order to provide quick positive changes in the driving current and maximum reproducibility.

While the bias field is held steady at each point, a 5 Kc/sec alternating field of amplitude of order 10^{-3} oersted is applied to measure the reversible susceptibility. A signal generator output passes in series through a high impedance, a non-inductive decade resistance box, and the core winding. A VTVM

is provided to measure voltage across either the decade box or the winding. The first serves to measure the current, proportional to the applied field, while the second measures the vector sum of the small IR drop in the winding and the induced voltage, proportional to the ac flux in the core. It is assumed that the induced flux is in phase with the current since other studies in this laboratory and elsewhere show that losses in ferrites are negligible at 5 Kc/sec.

The measured permeability is deduced from the ratio of these two voltages, although in practice the decade box is always adjusted to make the ratio unity to remove the dependence of the result on voltmeter calibration. The high impedance in series serves to make the current independent of the VTVM connections and of the value of the decade resistor. The signal generator is operated at low output level to assure a pure waveform. Further decrease of the signal voltage is found not to effect the value of the result, assuring that the signal is small enough to read the true limiting incremental permeability for zero applied field.

In these experiments the incremental field for measuring susceptibility is in all cases applied along the toroid by a toroidal winding. For the parallel case the bias field is applied in the same direction by means of another toroidal winding, while for the transverse case it is applied parallel to the toroid axis by means of an electromagnet.

When measuring the parallel susceptibility it is necessary to maintain an effective infinite impedance in the primary circuit to the measuring signal. This was accomplished by placing an iron core choke in series with the primary windings.

3.3 Parallel Case

3.3.1 Susceptibility. Discussion. The essential difficulties with this case arise from the fact that the magnetic field produced at a point within a

toroidal winding varies inversely with radius of the point from the toroid axis. So the magnetization and susceptibility vary with radius at given applied fields, and the observed values of these quantities are averages over the cross sectional area. Given the experimental values of the averages, it is not in general possible to solve explicitly for the unaveraged quantities to be compared with theory. Instead we must calculate geometrical averages of the theoretical curves, which can then be directly compared with the experimental data. However, we need to know how the magnetization varies with position in the sample to compute these averages. The only quantity whose geometrical dependence is known is the applied field H. We must make an additional assumption about the relation of M to H before the calculation can be done.

Thus we cannot make an ideal check of Eqs. 12 and 13 independent of any additional assumptions with data obtained from toroidal cores. However, it is found that average χ vs. M curves computed under several rather different simple assumptions for the dependence of M on H are similar in general features. In the following discussion, a compromise curve is arrived at which is believed to have qualitative validity.

Averaging Equations. In measuring magnetization, we measure a total flux $\phi = \int BdA = A\overline{B}$, where $\overline{B} = \frac{1}{A}\int BdA$ is the arithmetic mean of B. So if one defines $\overline{H} = \frac{1}{A}\int HdA$ and $\overline{M} = \frac{1}{4\pi}(\overline{B} - \overline{H})$, then

$$\overline{M} = \frac{1}{A}\int MdA = \frac{1}{(r_2 - r_1)}\int_{r_1}^{r_2} Mdr \qquad (17)$$

is the simple arithmetic mean of M over the cross section.

The averaging of susceptibility involves a weight factor. Experimentally we observe a ratio of two voltages. One is proportional to the average incremental ac induction amplitude $\overline{\Delta B}$, the other is proportional to the average incremental ac field amplitude $\overline{\Delta H}$. The observed average incremental permeability is thus not the average of the ratio $\Delta B/\Delta H$, but is the ratio of the averages $\overline{\Delta B}$ and $\overline{\Delta H}$.

So:

$$\bar{\mu}_\Delta = \frac{\overline{\Delta B}}{\overline{\Delta H}} = \frac{\int \Delta B dA}{\int \Delta H dA} = \frac{\int \mu \Delta H dA}{\int \Delta H dA} = \frac{\int \frac{\mu}{r}\, dr}{\int \frac{1}{r}\, dr} \tag{18}$$

since ΔH is proportional to $1/r$. Then trivially, the susceptibility

$$\overline{\chi_r} = \frac{1}{4\pi}(\overline{\mu_\Delta} - 1) = \frac{1}{4\pi}\left(\frac{\int \frac{\mu}{r}\, dr}{\int \frac{1}{r}\, dr} - 1\right) = \frac{\frac{1}{4\pi}\int \frac{\mu - 1}{r}\, dr}{\int \frac{1}{r}\, dr}$$

So

$$\overline{\chi} = \frac{1}{\ell n \frac{1}{\alpha}} \int_\alpha^1 \frac{\chi}{y}\, dy \tag{19}$$

where $\alpha = \frac{r_1}{r_2}$.

Theoretical Average Curves. Two extremely idealized assumptions for the dependence of M on H, which we believe bracket all our actual cases, are:

(A) Let the M-H loop be a parallelogram

$$\frac{M}{M_s} = \beta\left(\frac{H}{H_c} \pm 1\right) \quad \text{for} \quad -1 < \frac{M}{M_s} < +1$$

where M_s is the saturation magnetization, H_c the coercive force, and β is the ratio of the remanent magnetization to M_s.

(B) Let the M-H loop be a pair of laterally displaced Langevin functions

$$\frac{M}{M_s} = L\left[K\left(\frac{H}{H_c} \pm 1\right)\right]$$

where K is a constant.

Each assumption contains one parameter, which must be assigned some definite value in the calculations, and which is to be chosen to fit the ideal loop to some feature of actual ones. The ideal loops were fitted to the criterion that the remanent magnetization is $M_R \cong 0.2\ M_s$.

$$\beta = \frac{1}{5} \qquad \text{in (A)}$$

$$K = 0.615 \quad \text{in (B)}$$

Another parameter occurring in the calculations is the ratio $\alpha = r_1/r_2$. We take $\alpha = 1/2$ for definiteness, which is the nominal ratio for all of our cores.

Fig. 6 shows the averaged magnetization $\overline{M}/M_s$ vs. $\overline{H}/H_c$ for these two assumptions (solid lines). The approach to saturation of these two curves clearly represents opposite extremes to the general features of observed curves. For (A) the ideal relation itself (not averaged) is shown, where the averaged curve differs from it, by the dashed line. For (B) this difference is everywhere too small for the separate curves to be distinguished on this scale. The given curve is the averaged one, and the curve Δ represents the difference $\overline{M}/M_s - M/M_s$ on an expanded scale.

For each of these two assumptions we have calculated the integral χ/χ_o, Eq. 19 for several values of $\overline{H}/H_c$, using Eqs. 12 and 13. The results are plotted against $\overline{M}/M_s$, taken from Fig. 6, together with the ideal relation itself, in

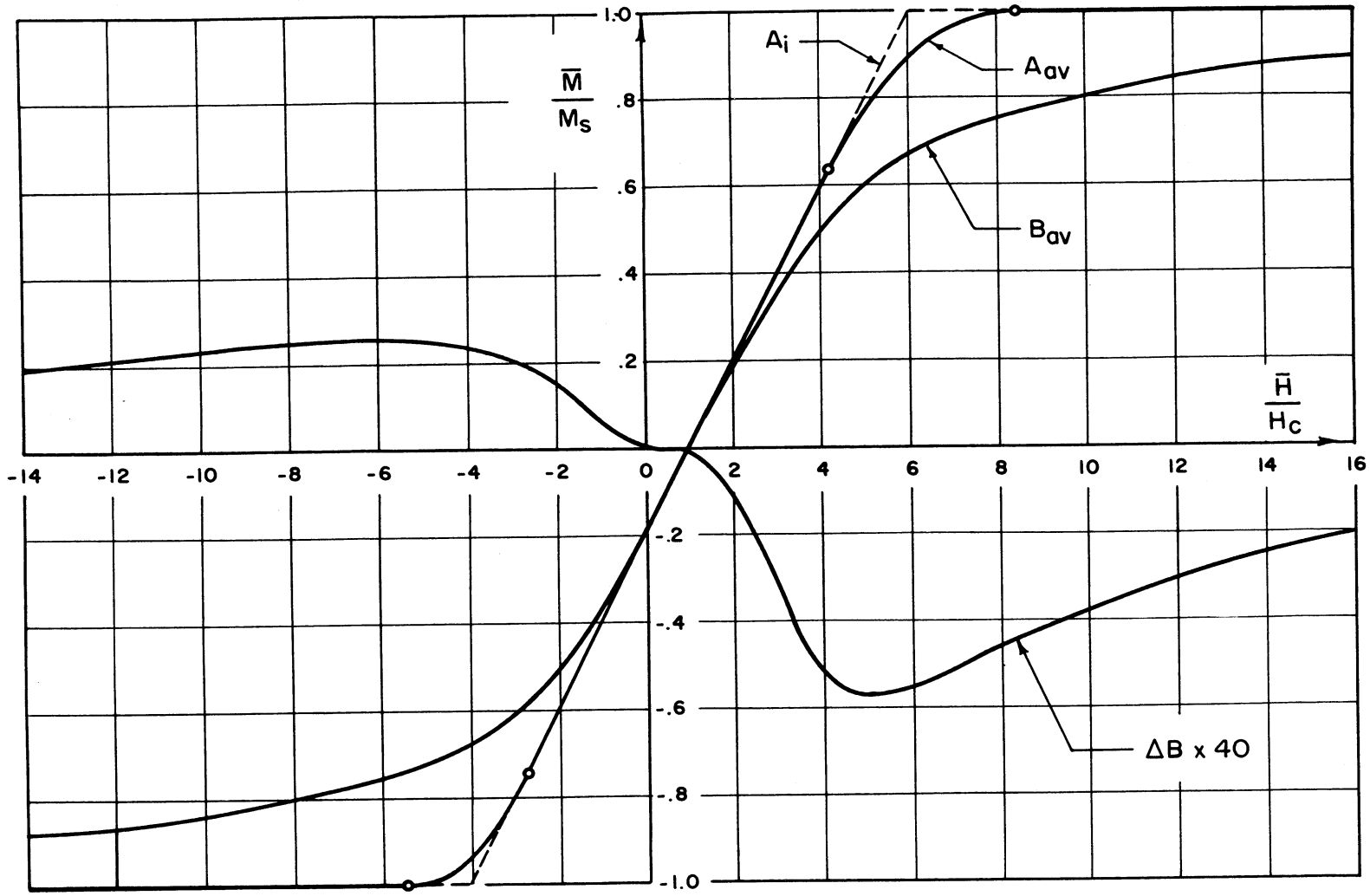

FIG 6
EFFECT OF TOROIDAL GEOMETRY ON M-H LOOP

A_i, B_i: IDEALIZED BEHAVIOR FOR INFINITE SPECIMEN
A_{av}, B_{av}: AVERAGED BEHAVIOR FOR TOROIDAL GEOMETRY
$\Delta B = B_{av} - B_i$

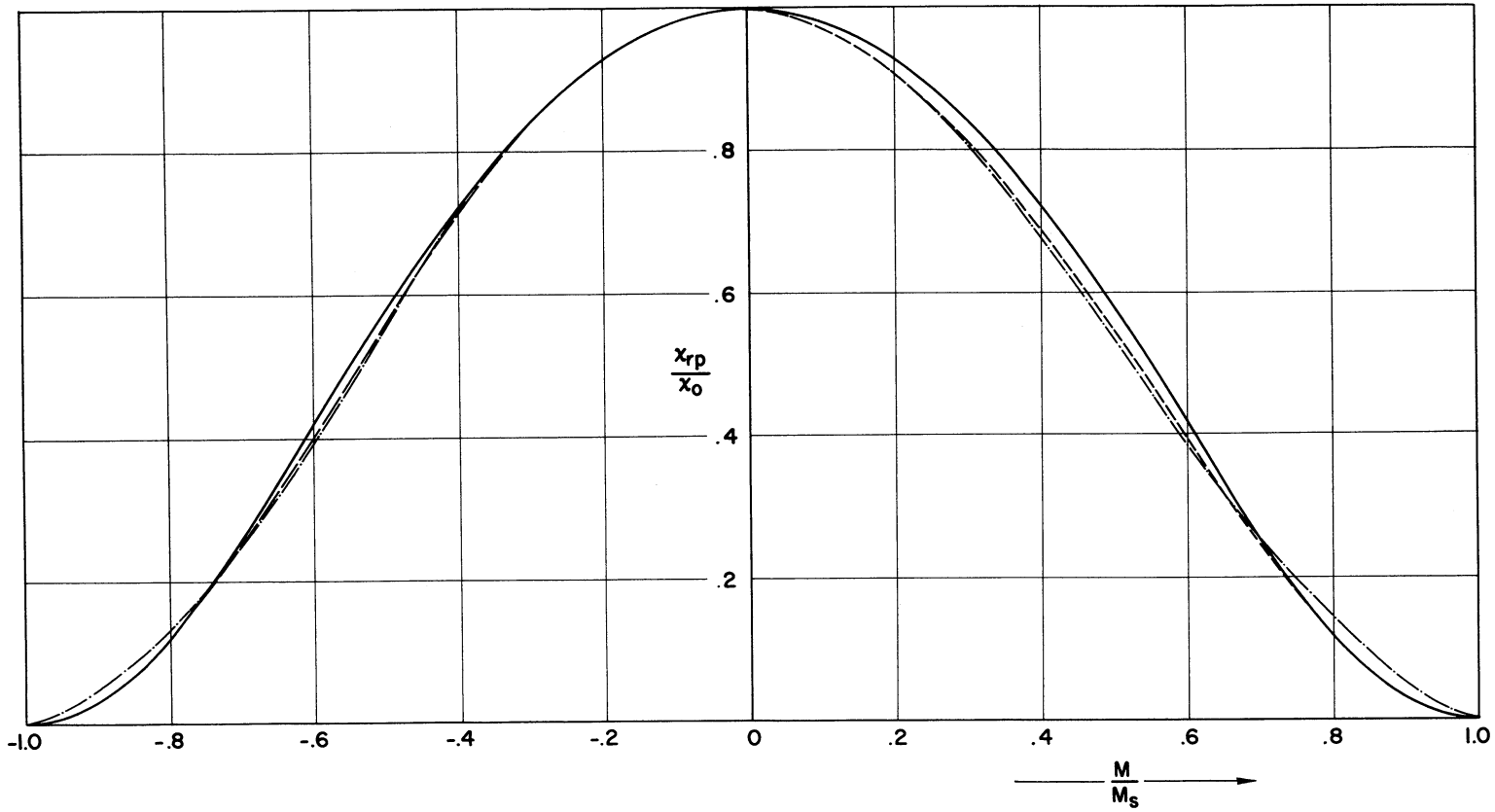

FIG 7

DISTORTION DUE TO TOROIDAL GEOMETRY

IDEAL CURVE ——

AVERAGE OVER TOROID

—— for $\frac{M}{M_s} = \frac{1}{5}\left[\frac{H}{H_c} - 1\right]$

------ for $\frac{M}{M_s} = L\left[.615\frac{H}{H_c} - .615\right]$

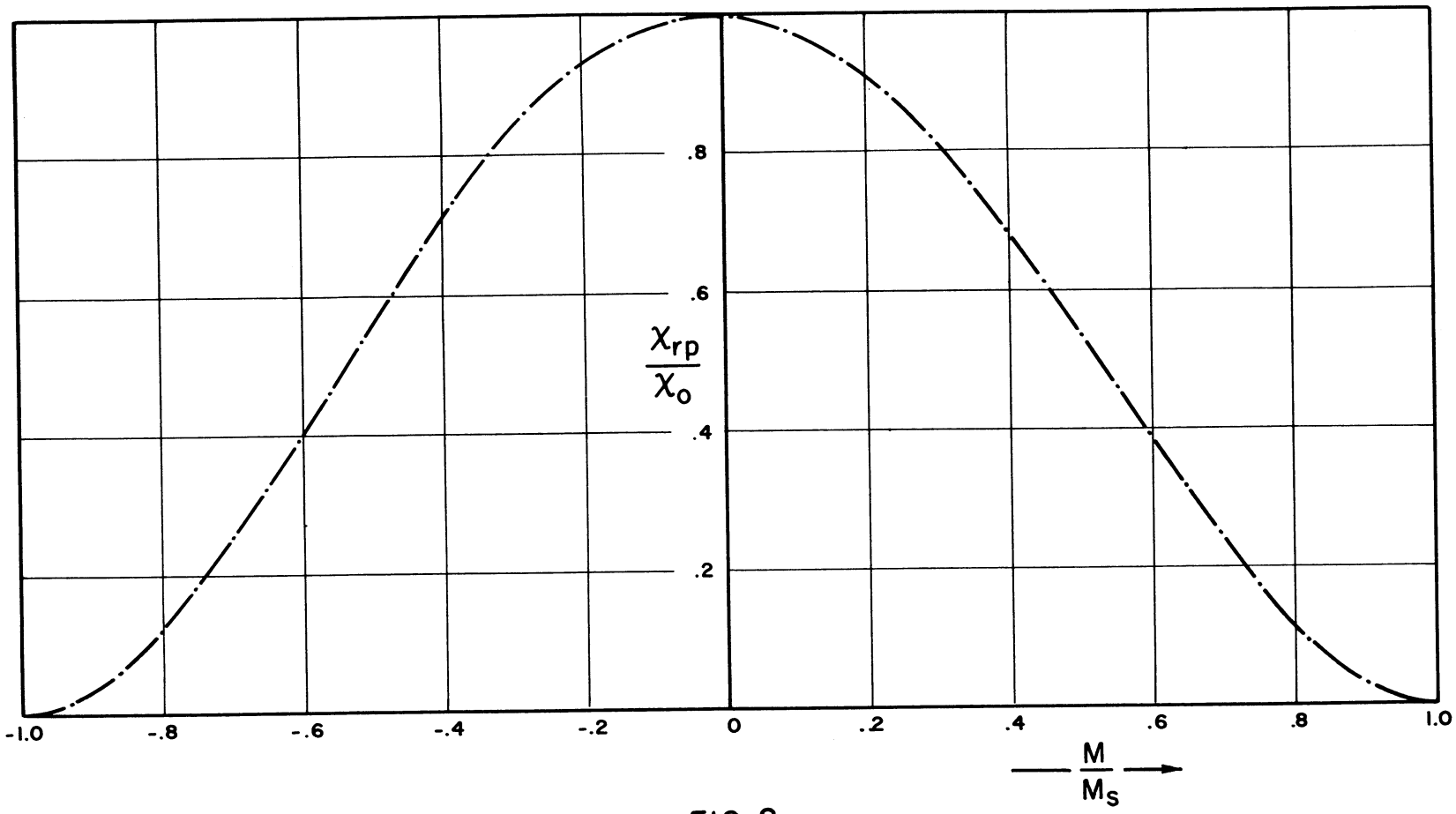

FIG 8

COMPROMISE CURVE FOR PARALLEL AVERAGES

Fig. 7. It is seen that the averaged curves each differ from the ideal curve in essentially similar respects.

The labor of preparing such a theoretical curve from an M vs. H curve especially fitted to each experimental case is felt to be excessive, since the integrals yield only to numerical methods. Since the results of these two extreme assumptions are so similar, it is felt that a "compromise" curve based on them has enough qualitative validity to suffice. Fig. 8 shows such a curve, and this is the "theoretical" curve presented for comparison with experimental data in all the graphs of Section 4.1.

3.3.2 Magnetization. The magnetization was measured in accordance with the description of Section 3.2. A special difficulty arises only for the measurement of the saturation magnetization. The measurement of the saturation magnetization is inherently difficult. It must be known for to compare the susceptibility curves with the theory it is necessary to normalize the magnetizations.

Our method of measuring M_s was to trace out the B-H loop to as high an applied field as could easily be applied around the toroid. This was about 225 oe. The data were corrected for the finite wire size of the B winding, then M_s was plotted against H. A Langevin function was fitted to the two highest points, and from this a value for M_s was calculated. This value is quoted in Section 4.1.

3.4 Transverse Case

3.4.1 Susceptibility. There is no a priori distortion of the susceptibility measurements in this case, even though they are made in the same direction and with the same toroidal windings as before. For now the bias field, which is applied parallel to the toroid axis by an electromagnet, is nominally uniform. The resulting magnetization is assumed to be essentially homogeneous so that the resulting susceptibility has a constant value throughout the sample. Therefore,

even though the incremental field ΔH still varies with radius the resulting incremental induction ΔB is everywhere proportional to it, and the ratio of their averages is the same as the ratio of their values at any point. Note that Eq. 19 reduces properly in agreement with this:

$$\overline{\chi} = \frac{\int \frac{\chi}{r}\, dr}{\int \frac{1}{r}\, dr} = \frac{\chi \int \frac{1}{r}\, dr}{\int \frac{1}{r}\, dr} = \chi \tag{20}$$

Accordingly, the theoretical curve appearing on all experimental plots for the transverse case is just that given by Eqs. 13 and 15.

3.4.2 Magnetization. Demagnetizing Factor. The essential difficulty of the transverse case is the measurement of the magnetization when a non-zero demagnetizing factor is present.

The true internal field H is the sum of the applied field H_a and the demagnetizing field NM, i.e., $H = H_a - NM$. As always, $4\pi M = B-H = (\mu-1)H$. Thus:

$$H = \frac{1}{1 + \frac{N}{4\pi}(\mu-1)} H_a = \frac{1}{\left(1 - \frac{N}{4\pi}\right)} \left[H_a - \frac{N}{4\pi} B\right] \tag{21}$$

and

$$4\pi M = (\mu-1)H = \frac{(\mu-1)\, H_a}{1 + \frac{N}{4\pi}(\mu-1)} \tag{22}$$

and for the apparent magnetization M_a, defined by $4\pi M_a \equiv (B - H_a)$ one obtains:

$$M_a = \left(1 - \frac{N}{4\pi}\right) M \tag{23}$$

When the "demagnetizing factor" $\frac{N}{4\pi}$ approaches unity, as for a thin disk magnetized normal to its area, and if μ is fairly large, then:

(a) From Eq. 21, $H_a \approx \frac{N}{4\pi} \mu H = \frac{N}{4\pi} B$. To produce a given field H in the sample will require an applied field many times larger, in fact of the same order of magnitude as B. Further, the true field may be essentially unknown experimentally because it is given as a small difference of large terms.

(b) Although Eq. 22 shows that the sample can still be magnetized by a sufficiently large applied field, the experimental apparent magnetization will approach zero according to Eq. 23.

For magnetization parallel to the axis our toroids appear as disks with a length/diameter ratio of 1/4 or less, for which the demagnetizing factor is approximately 0.8. However, if the field on the core is applied by an electromagnet whose pole faces are close to the core surface the effective demagnetizing factor becomes smaller and should ideally become zero if the pole faces make perfect magnetic contact with the core surface.

We have measured the apparent saturation magnetization of a core as a function of the electromagnet gap and found that it increased sharply as the gap approached zero. The curve became so steep that its limiting value at the ideal zero was rather indeterminate. Therefore this method is not suitable for the determination of saturation magnetization.

However, one sees from Eq. 23 that the ratio of the apparent magnetization M_a to the true magnetization M is given by $\left(1 - \frac{N}{4\pi}\right)$ which is assumed to be constant independent of field strength for a fixed geometry. Thus for a given point $\frac{M_a}{M} = \frac{M_{sa}}{M_s}$ where the subscript s denotes the saturation value. So, if the core is subjected to a given applied field one can determine the value of $\frac{M}{M_s}$ correctly

even though he has no idea what the true magnetization and true net field might be. If then one measured $\frac{\chi}{\chi_o}$ simultaneously, the plot of these pairs of value contains no dependence on the demagnetizing factor.

This simplification is, of course, subject to the assumption that N is actually constant so one should choose the geometry to keep N as small and the applied field as homogeneous as possible.

Measurement of Magnetization. The magnet used in these measurements was built with accurately parallel plane pole faces about 40% larger than the test cores and a continuously adjustable gap. The core windings are made flat and uniform, and the magnet gap is closed down so as to clamp the core in place. The windings on a test core are shown in Fig. 9.

The cores are provided with a girdle winding embracing the core cross section only, designated the "B" winding. A second flat winding on a teflon plug fits into the hole in its center and is called the H winding. The flux measured by the H winding, divided by its area and number of turns, is the measure of the applied field H_a. The B winding, although of No. 34 wire, actually embraces an area several percent larger than the core cross section. This area carries a flux density equal to H_a, and since H_a is of the same order as B this extra flux must be subtracted from the total measured by the B winding.

The driving current of the magnet is cycled about a given set of values, as described in section 3.2, while the flux changes in the B and H windings are separately measured by the fluxmeter. Then $4\pi M_a = (B - H_a)$.

The magnet is itself an iron system having some hysteresis and remanence so both the applied field H_a and the flux density B in the core will have certain remanent values $-\eta$ and $-\beta$ respectively as the driving current passes through zero while increasing. The fluxmeter gives the relative values $(H_a+\eta)$ and $(B+\beta)$ for

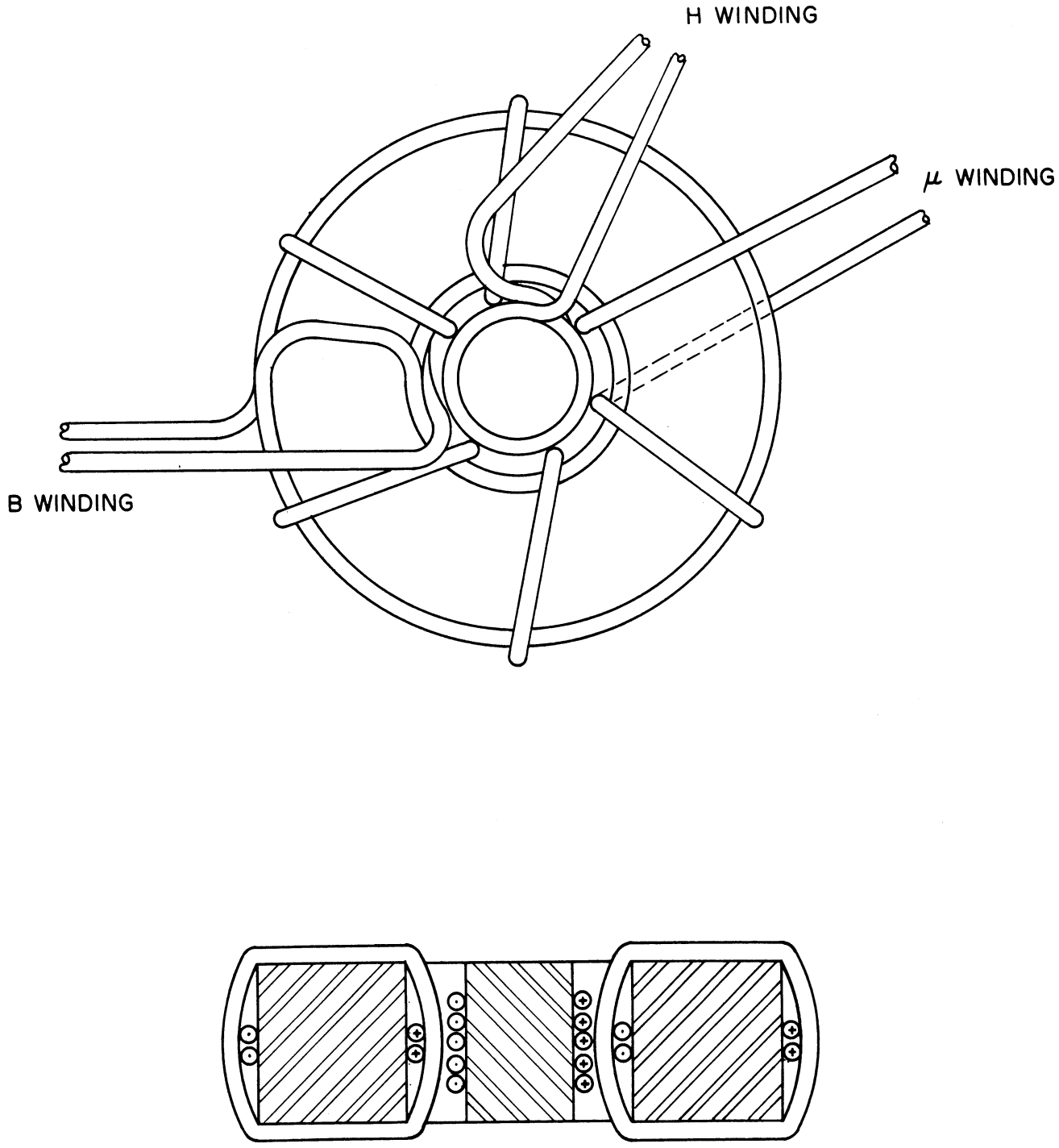

FIG 9

TEST CORE WINDINGS

each point of the loop, so the apparent M then also contains an additive constant ν.

$$(B + \beta) - (H_o + \eta_o) = 4\pi (M_o + \nu); \qquad 4\pi\nu = \beta - \eta_o$$

A typical core reaches saturation at several times smaller a field than does the magnet, so that the cycle of current values used is only a minor loop for the magnet itself. There is no assurance that this minor loop is symmetrical about the origin so the constants η and β are essentially not known without some absolute field measure. Any sort of probe to make such a measure would interfere with optimum geometrical arrangements. One can in principle evaluate ν by plotting a loop of M_a vs. magnet current extending to saturation in both directions and choosing the zero of M_a halfway between the two saturation values. However, it is more convenient in these experiments to evaluate it in the following way.

A plot of incremental permeability vs. magnetization gives in general a different curve, as M increases from zero to saturation along the major loop, from the curve obtained as M decreases from saturation to zero. These two curves necessarily meet and cross at M = 0 for the whole graph must by symmetrical in the two opposite directions of M. Thus the place where the "ascending" and "descending" experimental curves of μ_Δ cross each other identifies the zero of M.

The experimental procedure goes as follows. The magnet current is taken repeatedly around a fixed cycle of values, starting always at zero and using always the same peak values but stopping in between at successive intermediate values. Flux readings relative to the starting point are read from both the B and H windings for each of these intermediates with the fluxmeter, and χ_r is read at each point from the toroidal winding as in Section 3.2. The corrected difference of the B and H readings is $4\pi(M_a + \nu)$, obtained as a function of magnet current I.

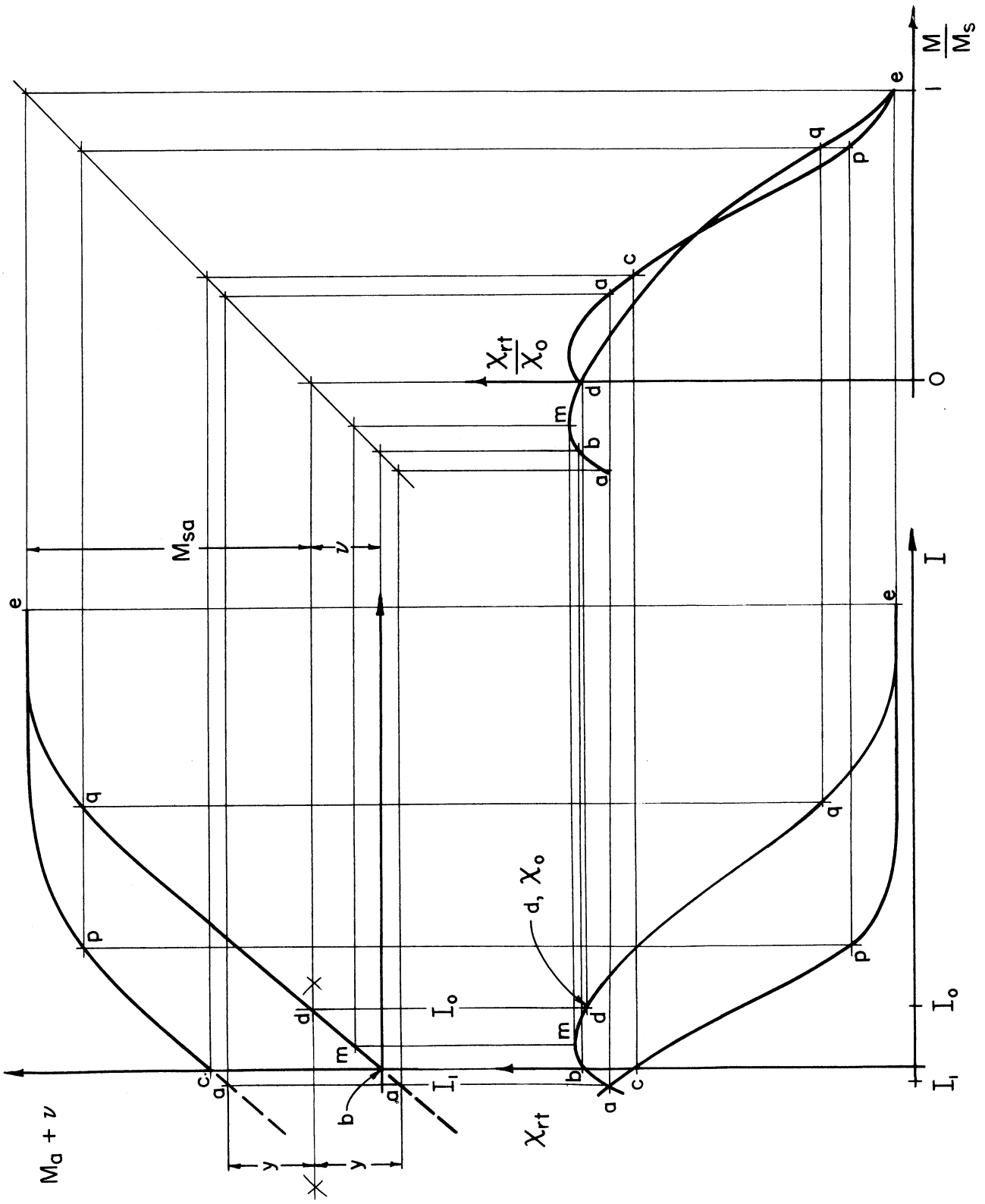

FIG 10

GRAPHICAL CONSTRUCTION $\frac{\chi_{rt}}{\chi_o}$ VS $\frac{M}{M_s}$

The data for χ_r is plotted vs. I to determine the current I_1 at which the two branches cross. The two values of $(M_a + \nu)$ for this current (one with ascending current, other with descending current) must then be equal but opposite in sign, which gives an equation for ν. One then determines from the data the value I_o of current at which M_a is zero on the ascending curve. The value of χ_r on the ascending curve at the current I_o is χ_o. M_{sa} is determined from the experimental value of $(M_a + \nu)_s$. The data are renormalized to give $\frac{M_a}{M_{sa}}$ and $\frac{\chi_r}{\chi_o}$, each vs. I. Finally these values are plotted against one other to give the result. Fig. 10 summarizes this procedure graphically. Note that points are obtained for only one sign of the applied field. We have measured points on the other side in a core or two as a check, and have found that the method of determining ν is valid.

4. EXPERIMENTAL RESULTS

4.1 General Properties.

Data were taken on three different ferrite specimens that were purchased from the General Ceramics and Steatite Corporation, Keasby, New Jersey, and represent their types E, G, and I. Room temperature data only are given on cores G-5 and I-8, data at about room temperature and at 25° intervals to 100° C on core E-3.

A summary of the measured values is given in Table III.

H_c is the coercive force in oersteds, H_c' is that applied field at which the parallel susceptibility attains its maximum value. H_c' is always of the same sign as, but is always less than H_c. Values of H_c, H_c' and remanance M_r/M_s are given for measurements around the toroid. It would have been desirable to know H_c' for the transverse susceptibility but unfortunately our data does not yield this information.

TABLE III

MAGNETIC PARAMETERS OF E-3, G-5, and I-8

		Parallel						Transverse		
Sample	Temperature °C	H_c oe	H_c' oe	$\frac{M_r}{M_s}$	M_s cgs	χ_o	χ_{max}	M_s^a cgs	χ_o	χ_{max}
I-8	25	.115	.081	.371	216	89.8	94.4	177	84.4	86.4
G-5	25	.260	.22	.383	270	30.5	31.0	214	29.1	30.2
E-3	25	.595	.38	.431	294	37.0	39.3	296	37.1	37.5
	50	.590	.48	.377	261	40.6	41.9	263	39.4	40.0
	75	.524	.30	.342	232	40.7	43.2	236	41.4	42.0
	100	.467	.30	.325	207	41.7	44.2	206	42.4	43.0

4.2 Susceptibility versus Magnetization.

A sample curve showing $4\pi(M_a + \nu)$ versus current applied to the electromagnet is shown in Fig. 11 for the transverse field measurements. The value of M_{sa} is obvious from the figure.

The experimental curves showing the variation of the reversible susceptibility with magnetization for both parallel and transverse fields are shown in Figs. 12 thru 18. Fig. 18 is a replot of Fig. 12 and the χ_{rp} vs. H curve from which Fig. 12 was plotted. The solid lines represent the experimental data, the dashed lines the theoretical curves.

It is to be noted from Figs. 12 thru 17 that the maximum value of both susceptibilities occurs for decreasing |M| before M reaches zero. Except for the region of the maximum the experimental curve is lower than the theoretical curve.

Fig. 18 is plotted to emphasize that the parallel susceptibility always has a larger value for decreasing than for increasing |M|. On the contrary there is a crossover in the transverse susceptibility loop, the curve for decreasing|M| being higher at low fields and lower at high fields.

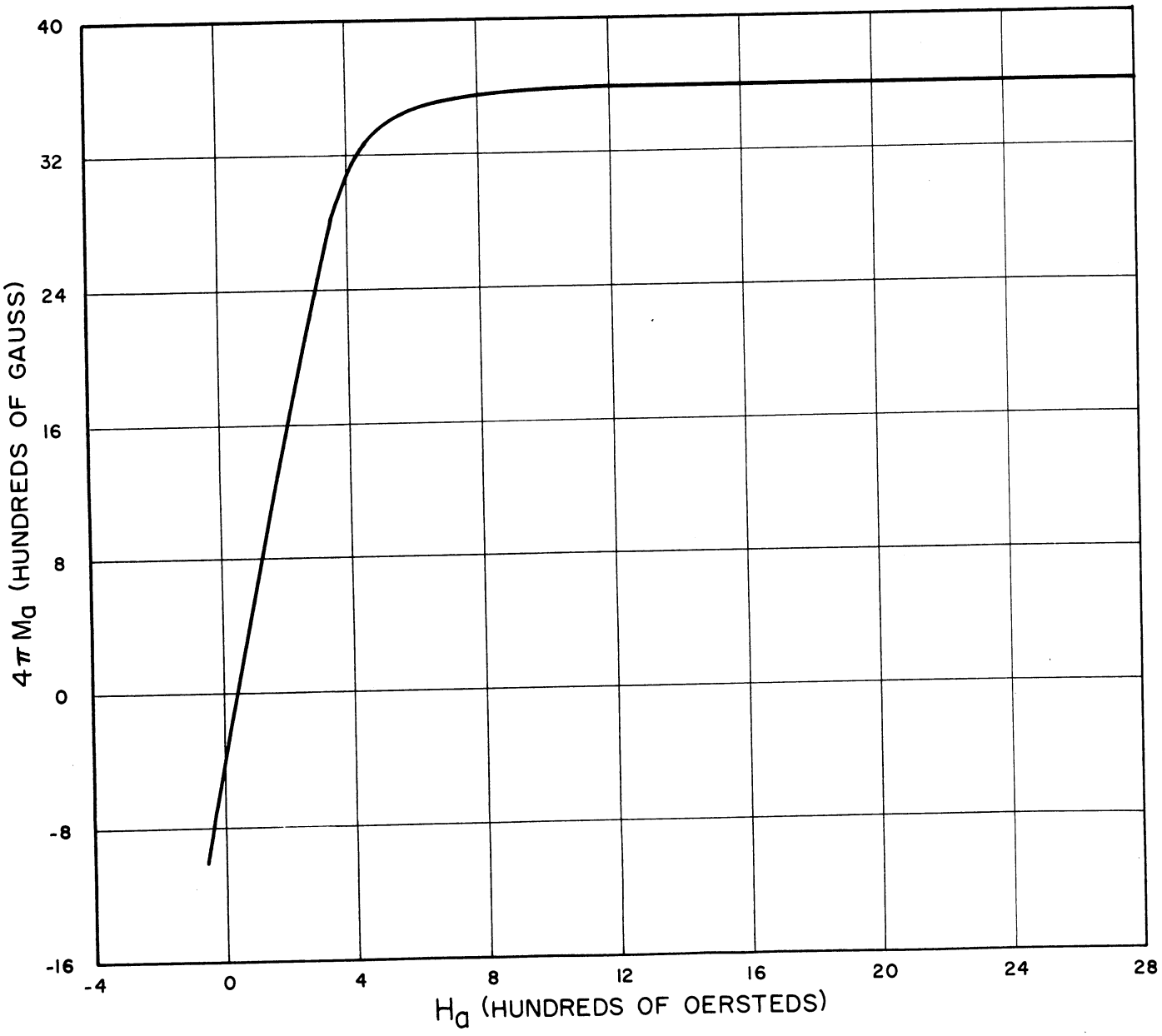

FIG 11
SAMPLE TRANSVERSE MAGNETIZATION CURVE

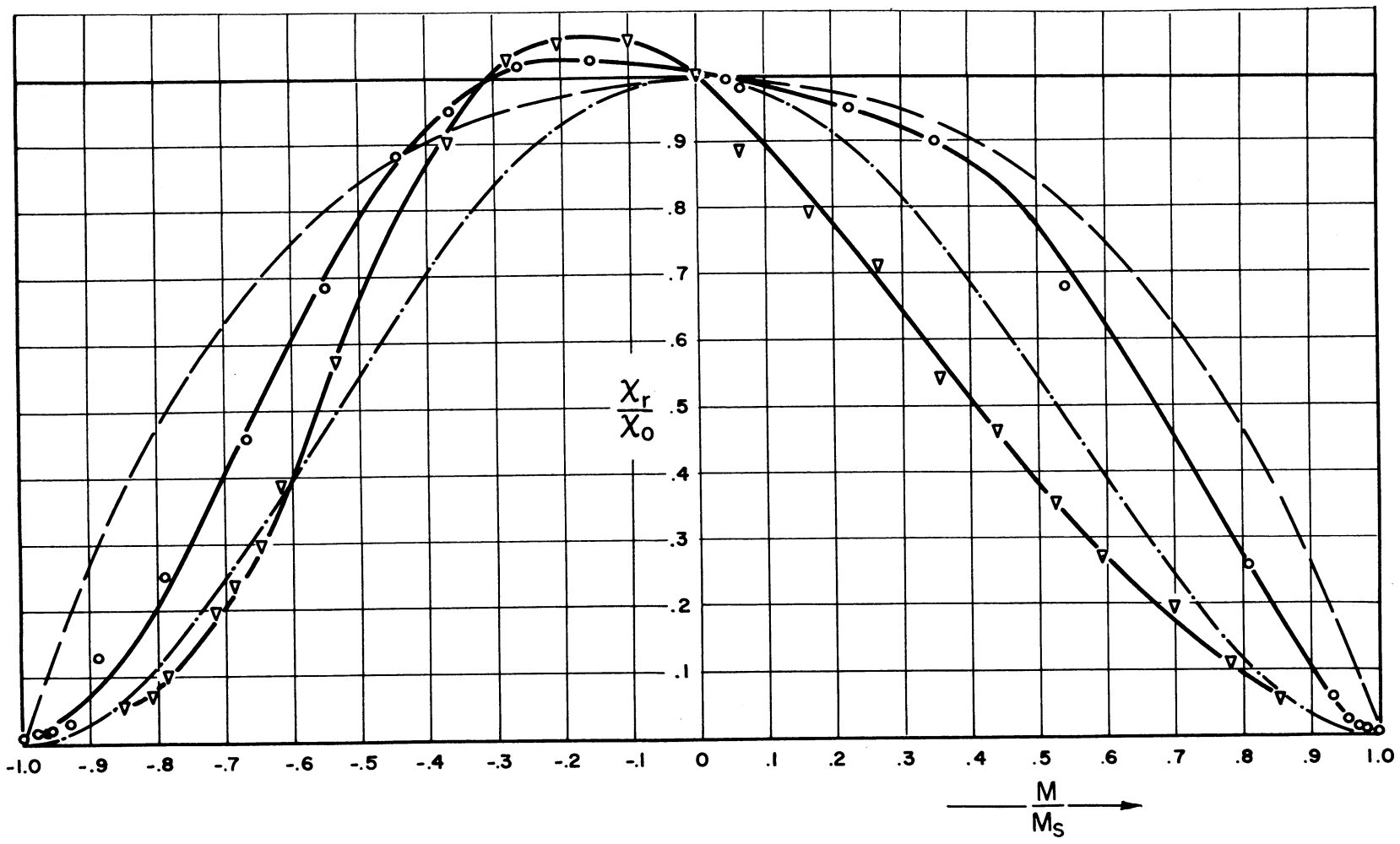

FIG 12

REVERSIBLE SUSCEPTIBILITY VS MAGNETIZATION

EXPERIMENTAL { o——o TRANSVERSE ; ▽——▽ PARALLEL

THEORETICAL { — — TRANSVERSE ; —·— PARALLEL

GC-1-8; 25°C

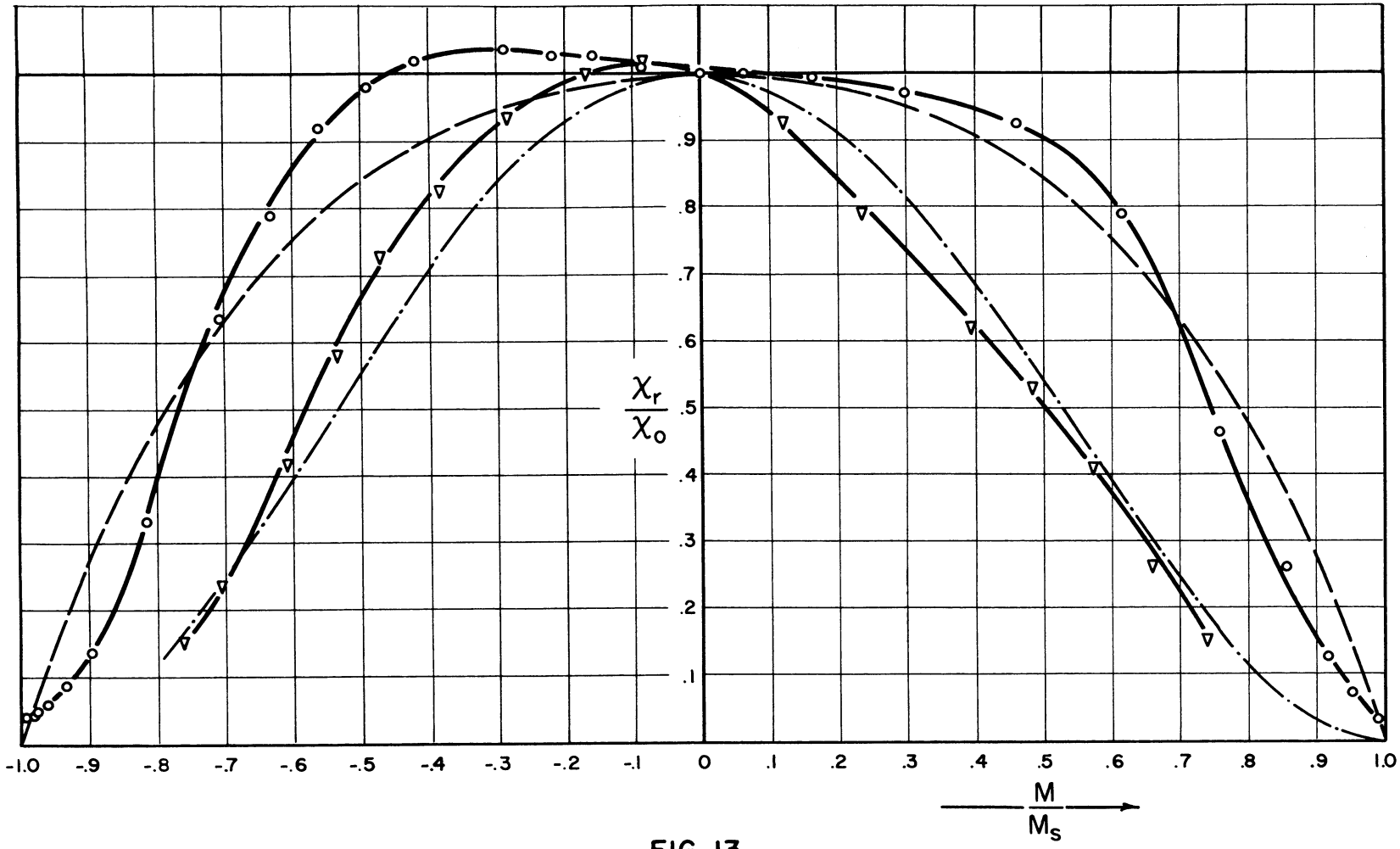

FIG 13

REVERSIBLE SUSCEPTIBILITY VS MAGNETIZATION

GC-G-5; 25°C

EXPERIMENTAL { o——o TRANSVERSE ▽——▽ PARALLEL

THEORETICAL { — — TRANSVERSE —·— PARALLEL

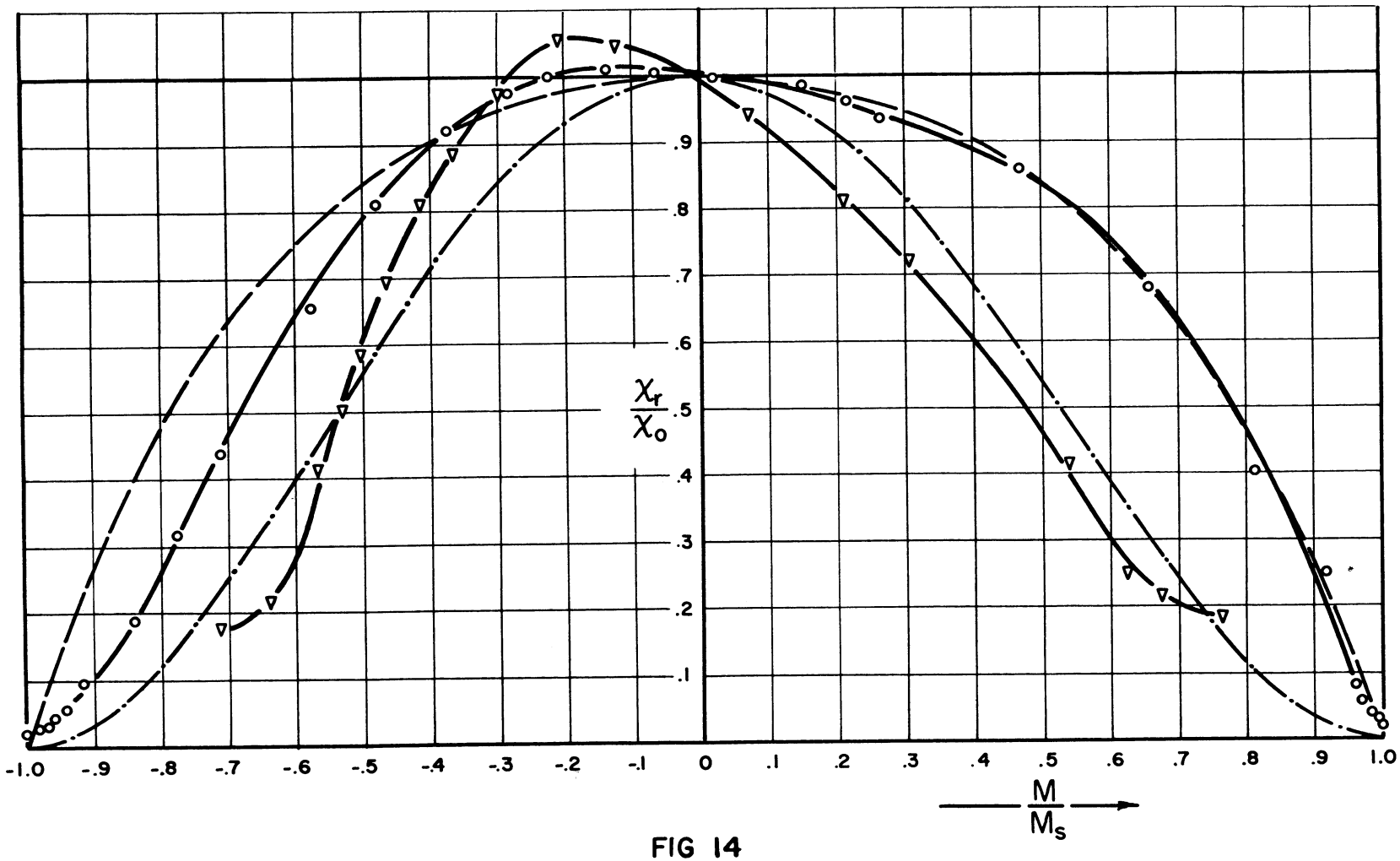

FIG 14
REVERSIBLE SUSCEPTIBILITY VS MAGNETIZATION

EXPERIMENTAL { TRANSVERSE, PARALLEL
THEORETICAL { TRANSVERSE, PARALLEL

GC-E-3; 25°C

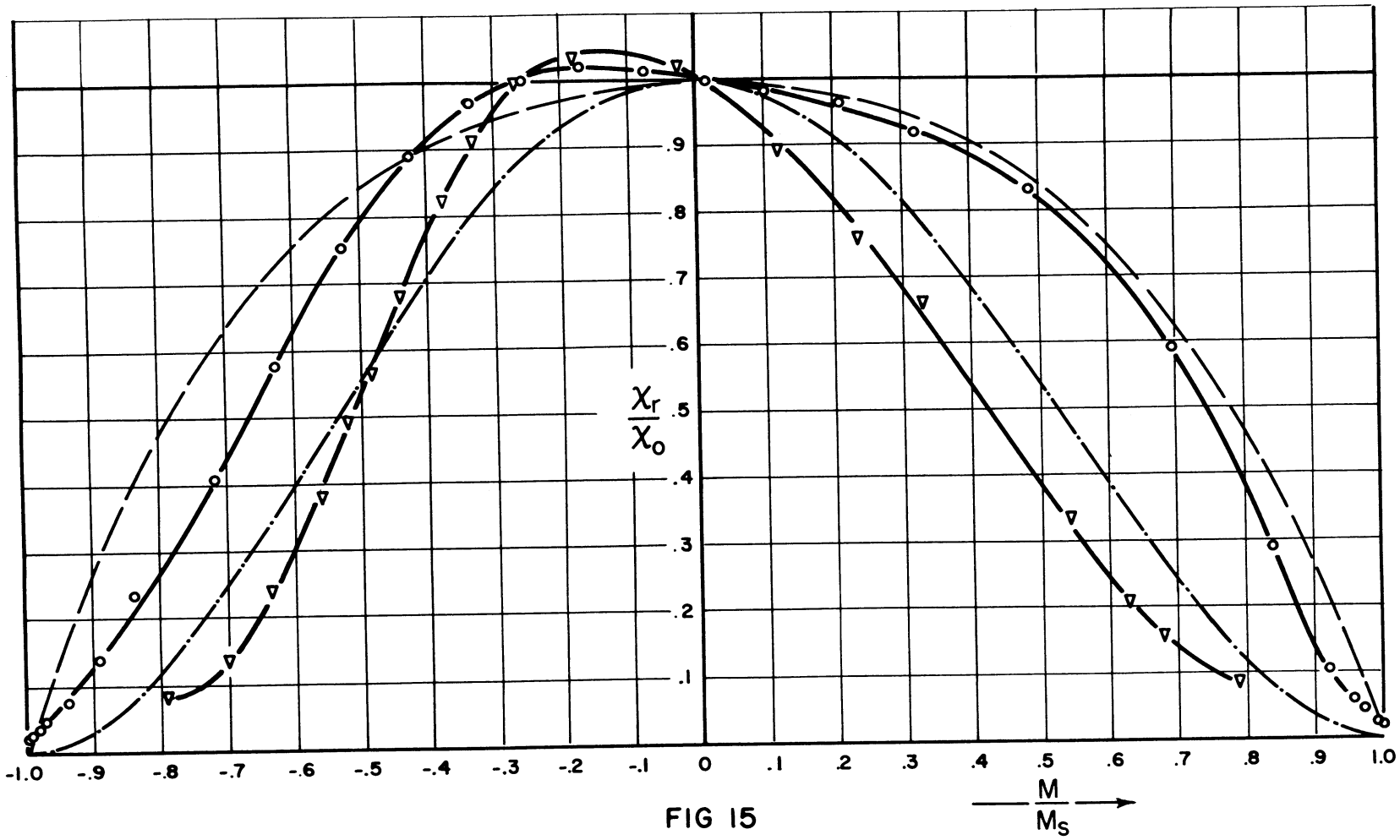

FIG 15

REVERSIBLE SUSCEPTIBILITY VS MAGNETIZATION

EXPERIMENTAL { o——o TRANSVERSE ; ▽——▽ PARALLEL

THEORETICAL { — — TRANSVERSE ; —·— PARALLEL

GC-E-3; 45°C

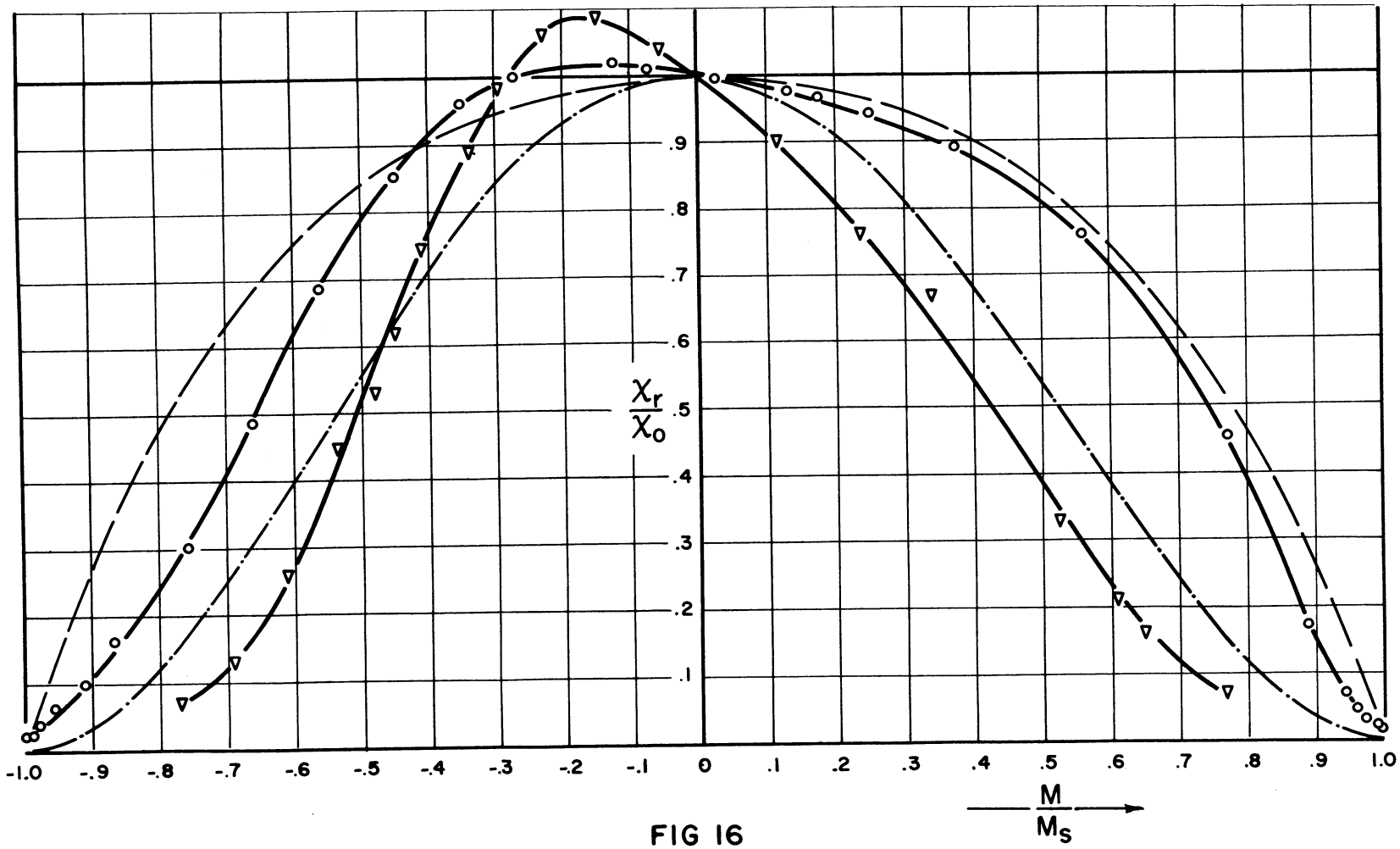

FIG 16
REVERSIBLE SUSCEPTIBILITY VS MAGNETIZATION

EXPERIMENTAL { o——o TRANSVERSE
▽——▽ PARALLEL

THEORETICAL { —— TRANSVERSE
—·— PARALLEL

GC-E-3; 75°C

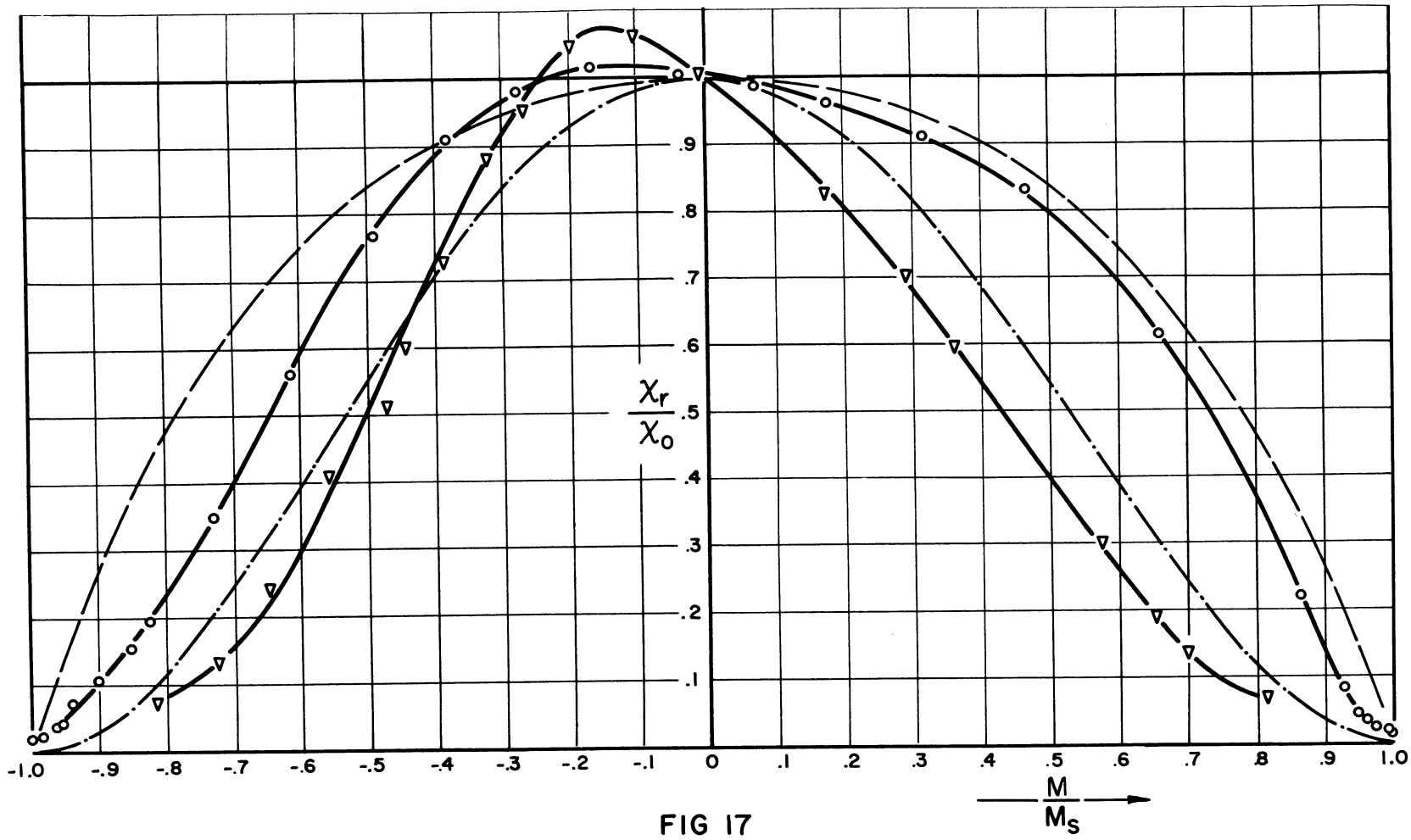

FIG 17

REVERSIBLE SUSCEPTIBILITY VS MAGNETIZATION

EXPERIMENTAL { o——o TRANSVERSE ; ▽——▽ PARALLEL

THEORETICAL { — — TRANSVERSE ; —·— PARALLEL

GC-E-3; 100°C

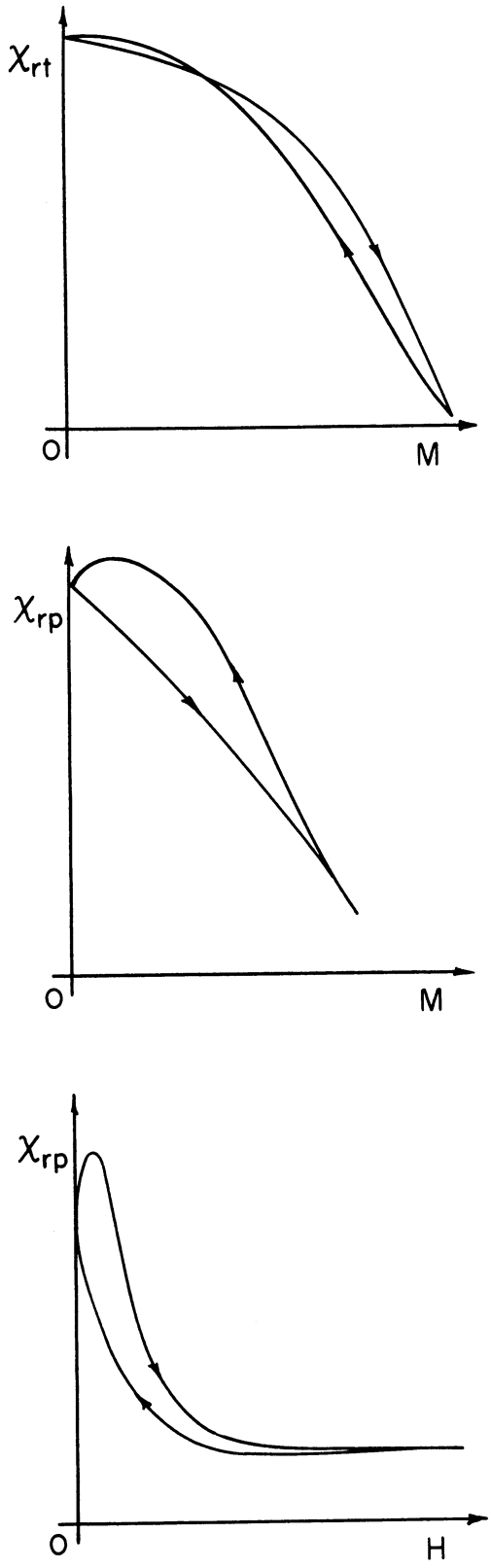

FIG 18

COMPARISON OF SUSCEPTIBILITY LOOPS
CORE E-3

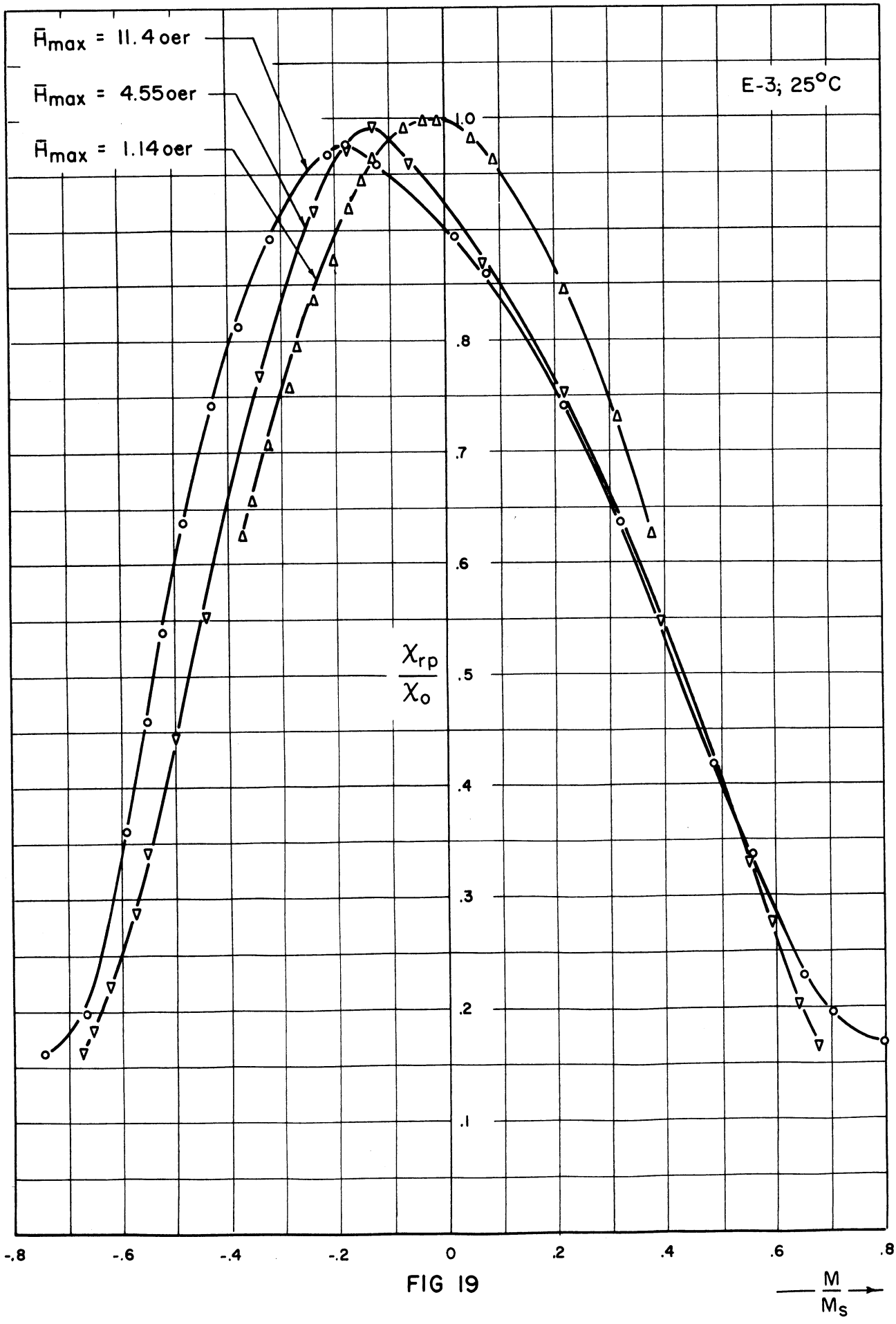

FIG 19

χ_{rp}/χ_o VS M/M_s FOR DIFFERENT PEAK MAGNETIZATIONS

Fig. 19 shows the variation of the maximum value of χ_{rp}/χ_o vs. M/M_s with the peak value of M reached during the cycling process. Similar curves are available for both I-8 and G-5. The peak value of susceptibility increases and shifts toward zero M as the peak M is diminished.

4.3 Errors

The accuracy of our susceptibility measurements was limited by the noise reading on our instrument for measuring the voltage drop across the toroid, (Hewlett Packard 400C VTVM) and our ability to read the meter. The normalized data are considered accurate within $\pm$ 5%, the absolute values accurate within $\pm$ 8%.

With the exception of the parallel field measurement of M_s, our magnetization data are limited in accuracy by fluxmeter drift and errors in meter reading. These are considered to be well within $\pm$ 5%.

It is difficult to estimate the error in the value gotten for M_s from fields applied around the toroid. This value must never be less than the value read from the transverse measurements. Table III shows the parallel measurement to be larger for G-5 and I-8 and the same for E-3 as the apparent value along the toroidal axis. The curves for χ_{rp}/χ_o vs. M/M_s should approach zero at $M = M_s$. That they do so would indicate our measurement would probably be within 10%.

5. EXTENSION OF THEORY

5.1 General Discussion

For a perfect single crystal with zero demagnetizing factor the application of a small field parallel with an easy direction of magnetization should result in an infinite susceptibility. That the susceptibility is noninfinite in polycrystalline material can be considered to be the result of two different types of forces acting to retard wall movements. These are reversible and irreversible forces.

In polycrystalline material the reversible forces can be considered as arising from intragranular potential minima and from intergranular demagnetizing factors. In the discussion of section 2.1 we described the forces as arising from some potential energy function that was a continuous function of spatial coordinate.

We now wish to discuss hysteresis and susceptibility using statistical arguments to describe the trapping of domain walls in potential holes, i.e. in metastable positions. Each hole is to be characterized by a single number, loosely called its "depth" f. A wall encountering such a hole will be trapped and assumed to be held rigidly if the total net force of the field plus reversible forces on the wall is less than f, but will break free if this force exceeds f. Actually these potential minima must surely, for finite wall areas, have a finite radius of curvature. However, for purposes of this discussion we consider them to be infinitely sharp i.e. the walls held rigidly when under the influence of a potential hole. A wall thus rigidly held in an infinitely narrow hole would contribute nothing to the susceptibility. The behaviour of a ferromagnet must lie somewhere between this model and the model assuming only reversible behaviour.

The magnitude and direction of the reversible forces arising from localized demagnetizing factors on a particular grain will depend upon the size, shape and neighbors of that grain. This will be rather independent of the magnetization of the material and must surely be distributed in some random fashion. Although the exact nature of this force distribution is not known its resulting variations in energy magnitude with direction must be nearly the same as for other reversible cases so the resulting distribution of magnetic moments throughout the material must approximate that given by an extremum of Eq. A1. This equation is very stable with respect to different force distributions as can be seen by

observing that in the neighborhood of the extremum value given by $\partial \ell n\, W/\partial N_\gamma = 0$ higher derivations of $\ell n\, W$ with respect to N_γ form a polynomial in negative powers of N_γ.

An illustration of the stability of this equation would be to apply the equations for isotropic material to $\left[111\right]$ material as discussed in section A.3. The equality to high values of η can be directly attributed to the slowly varying character of Eq. A1.

We therefore consider the distribution of magnetic moments in a ferromagnetic material when only reversible forces are applied to be described by Eq. A6. The resulting magnetic disorder could be considered as analogous to a magnetic entropy, and should be considered when dealing with magnetic energy problems.

5.2 The Irreversible Magnetization

In the appendix a quantity n_γ was defined as the number of domains of fixed and equal volume whose moments are oriented in the γ direction. Since we are now speaking of domain wall movement, this definition is no longer applicable. In this section n_j will be the fraction of the total number of atoms whose permanent dipole moments are oriented in the direction of the unit vector $\hat{\gamma}_j$.

If no potential holes or "snags" were present, then under an applied field H according to the reversible equations:

$$n_j = \frac{e^{AM_s(\vec{H}\cdot\hat{\gamma}_j)}}{\sum_i e^{AM_s(\vec{H}\cdot\hat{\gamma}_i)}} \tag{24}$$

In terms of wall positions, this must also be equal to (See Fig. 20)

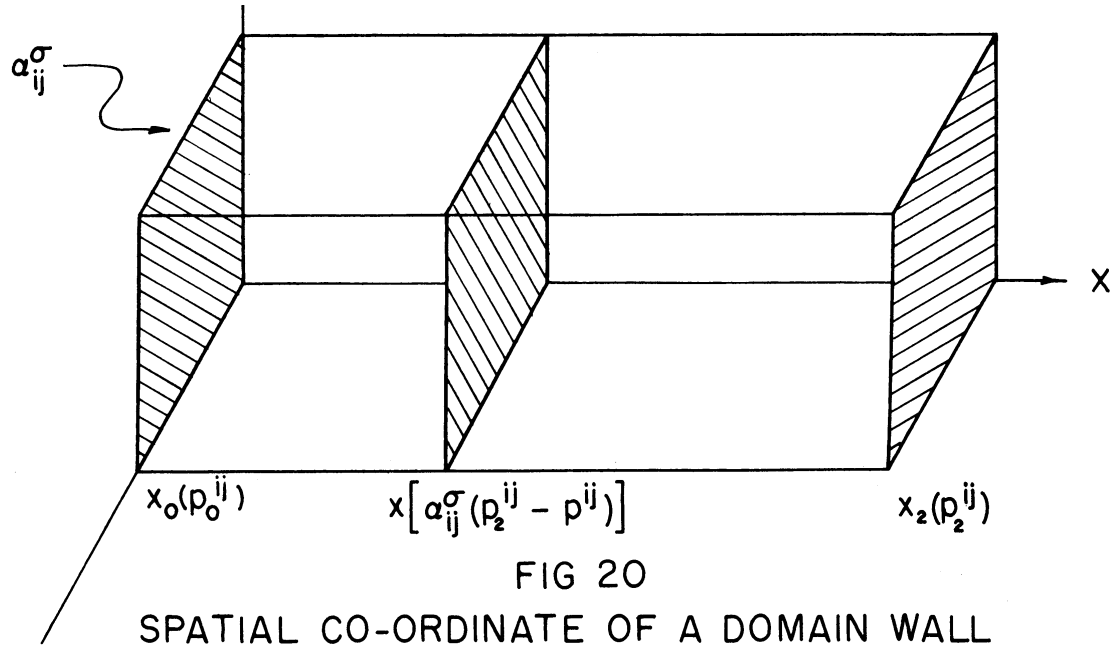

FIG 20
SPATIAL CO-ORDINATE OF A DOMAIN WALL

$$n_j = \frac{1}{\sum_i \gamma_i^2} + \sum_i \sum_{\sigma} a_{ij}^{\sigma} x^{\sigma} \tag{25}$$

a_{ij}^{σ} is the area of a particular wall separating domains oriented in the directions $\hat{\gamma}_i$ and $\hat{\gamma}_j$ respectively, x^{σ} is the spatial coordinate of the wall relative to a position at which the total net magnetization is zero and Eq. A1 is an extremum and $\sum_{\sigma}$ is a sum over all walls of type ij in unit volume.

If there were no snags, x would be a function only of the pressure which the applied field exerts on the walls. This pressure is given by

$$p^{ij} = M_s \left[\vec{H}\cdot(\hat{\gamma}_i - \hat{\gamma}_j)\right] \tag{26}$$

A given wall would find an equilibrium position for which the reversible forces just balanced this pressure.

When snags are present walls may become caught in them, and x is no longer a simple function of pressure. We can express the average x for a large

number of walls in terms of the distribution of these snags by arguments of the nature of a "mean free path" discussion.

Let the number of snags per unit volume whose depth, in the sense of section 5.1, lies between f and f + df be given by $\xi(f)$. The total number of snags per unit volume is then

$$Z = \int_0^\infty \xi(f)df$$

Suppose that initially there is a field $\vec{H}_0$ present, and that all the walls occupy positions x_0 determined only by the reversible forces and the field. That is, none of the walls are held in metastable positions. We will focus attention only on those walls of a particular class ij with area a_{ij}^σ lying in a particular range between a and a + da. When the field is changed to $\vec{H}_2$, each wall will tend to move to a definite new equilibrium position x_2. As it moves toward x_2, there is at each intermediate position x a net force f(x) of the field plus reversible forces, this force diminishing to zero when x_2 is reached.

According to the assumed model, if at x a wall encounters a snag bigger than f(x) it will be held there. If there are N_0^σ walls in the group considered, which we imagine to start moving together over the interval x_0 to x_2, the number $N^\sigma(x)$ still free to move at a position x in the interval will be diminished by the number so far caught. Thus we can write

$$dN^\sigma(x) = -N^\sigma(x)\, a_{ij}^\sigma\, dx \int_{f(x)}^\infty \xi(f)\, df$$

Upon integrating:

$$N^{\sigma}(x) = N_o^{\sigma} \exp\left[-a_{ij} \int_{x_o}^{x} dx' \int_{f(x')}^{\infty} \xi(f)\, df \right]$$

The fraction of the original group of walls which become snagged in the interval between x and x + dx is given by:

$$\Psi^{\sigma}(x)\, dx = \frac{|dN^{\sigma}(x)|}{N_o^{\sigma}} = \left[\exp\left(-a_{ij}^{\sigma} \int_{x_o}^{x} dx' \int_{f(x')}^{\infty} \xi(f)\, df \right) a_{ij} \int_{f(x)}^{\infty} \xi(f)\, df \right] dx$$

The average position $\bar{x}^{\sigma}$ at which the group of walls considered will become snagged when the field is changed to $\bar{H}_2$ is then:

$$\bar{x}^{\sigma} = \int_{x_o}^{x_2} x \, \Psi^{\sigma}(x)\, dx \qquad (27)$$

This average value of x is the quantity to be substituted into equation (25) when snags are present.

Eq. 24 is used to predict the magnetic properties of our experimental system. If we define a vector $\vec{H}'$ for which there is an equation analogous to 24 but which corresponds to a system described by $\bar{x}$ of Eq. 27 substituted into Eq. 25 , it is apparent that $\vec{H}'$ must have properties different from that of H. The product $\vec{H} \cdot \hat{\gamma}_j$ determines the fraction of the atoms with their moments oriented in the $\hat{\gamma}_j$ direction. Using Eq. 27 a different fraction of the atoms will have their moments oriented in the $\hat{\gamma}_j$ direction because of the dependence of $\Psi^{\sigma}(x)$ on direction. Therefore if $\vec{H}'$ is to be considered as a vector it must be considered as a special type of vector whose magnitude will be given by $|H|\, g(j)$ where g(j) is some function of the angle the field makes with the atoms in question.

It would be possible to describe this same phenomenon in terms of a different distribution function rather than a variable $\vec{H}$. Either of these methods would be quite involved. A third alternative is to describe this redistribution in terms of a different anisotropy type. This is done in the next two sections.

5.3 Modifications of the Reversible Model

5.3.1 Contribution of Metastable Volume. It was seen in section 5.1 that the reversible susceptibility of a ferromagnetic material is decreased by the presence of intragrain potential holes which are occupied by domain walls. In general these holes would have a finite radius of curvature. The greater the depth of a minimum the smaller is this radius, and therefore the less a wall occupying it will contribute to the susceptibility. This would always act to decrease the susceptibility from the value given by the reversible equations. This decrease from maximum should increase as the peak M reached during a cycle increases causing walls to cross potential barriers capable of retaining them in deep metastable states when the applied field is decreased. In general it would not be the same holes that would decrease the two different susceptibilities.

5.3.2 High M/M_s, decreasing $|M|$. When $|M|/M_s = 1$ all the material is necessarily aligned with the applied field. As $|M|$ is decreased from M_s the metastable volume will be predominately oriented in the direction of the macroscopic magnetization, the remainder we take to be oriented in accordance with the reversible equations. Thus at a specified value of η the number of atoms with their magnetic moments parallel with the biasing field will be increased by the action of the potential holes. Therefore for a specified value of M there will be more atoms aligned parallel than would otherwise be the case. This necessarily means the component antiparallel with the field is correspondingly increased. Since the number of atoms is fixed this must also mean that there

will be fewer atoms with their moments aligned normal to the field than would be the case with only reversible forces.

To find qualitatively how this affects the susceptibilities consider the extreme case of all magnetic moments oriented either parallel or antiparallel with the field. Eq. A7 then becomes:

$$\frac{M}{M_s} = \frac{e^{AM_sH_r} - e^{AM_sH_r}}{e^{AM_sH_r} + e^{-AM_sH_r}} = \tanh \eta$$

where, as usual, $\eta = AM_sH_r$.

This leads to:

$$\frac{\chi_{rp}}{\chi_o} = \operatorname{sech}^2 \eta; \qquad \frac{\chi_{rt}}{\chi_o} = \frac{\tanh \eta}{\eta} \qquad (28)^*$$

Values of χ_{rp}/χ_o and χ_{rt}/χ_o vs. M/M_s are given in Table IV. The result is that both curves are higher than the corresponding curve for isotropic material, but are of the same order and of the same general form.

TABLE IV

M/M_s and χ_r/χ_o vs η for $f(\eta) = \tanh \eta$

η	$\tanh \eta = M/M_s$	$\operatorname{sech}^2 \eta = \chi_{rp}/\chi_o$	$\frac{1}{\eta} \tanh \eta = \chi_{rt}/\chi_o$
0	0	1	1
.3	.291	.914	.971
.6	.537	.711	.895
.8	.664	.559	.830
1.0	.762	.420	.762
1.4	.885	.216	.632
2.0	.964	.071	.482
5.0	.9999	.000	.200
∞	1.000	0	0

* The integration constant in χ_{rt}/χ_o must be zero for symmetry to exist about $\eta = 0$.

5.3.3 High M/M_s, increasing $|M|$. In a randomally oriented state none of the volume is in a metastable condition. After the application of an external field a finite fraction of the material will be maintained in metastable positions. Since domain walls would move the farthest when located between atoms with moments parallel and antiparallel with respect to the field a larger fraction of the material oriented antiparallel will be held in metastable states than in any other direction. This fraction decreases to zero for parallel alignment. As the magnetization increases the amount of material available to be held in these metastable states is smallest for antiparallel and increases to maximum at parallel alignment. As a result one would, for high values of M/M_s, expect the total number of atoms whose magnetic moments are held in metastable conditions to go through a maximum at some angle between 0 and π radians. Thus for a specified η the normal component of magnetization will be increased. It then follows that for a specified M the total magnetic moment both parallel and antiparallel with the field must be decreased but the difference remains the same, so the fraction of the atoms antiparallel must decrease.

The extreme condition of this model would be for this fraction to be zero, i.e. no atoms possess magnetic moments which make angles of greater than $\pi/2$ with the applied field. For this case the magnetization would be given by: (See section A.2)

$$\frac{M}{M_s} = \frac{\int_0^1 \gamma \, d\gamma \, e^{\eta\gamma}}{\int_0^1 d\gamma \, e^{\eta\gamma}}$$

where:

$$\gamma = \cos\theta$$

$$\eta = AM_sH_r$$

This leads to:

$$\frac{M}{M_s} = \left[\frac{e^{\eta}}{e^{\eta}-1} - \frac{1}{\eta} \right]$$

For small fields,

$$\frac{M}{M_s} = \frac{1}{2} + \frac{\eta}{12} + \cdots\cdots\cdots$$

The resulting susceptibilities are given by:

$$\frac{\chi_{rp}}{\chi_o} = 12 \left[\frac{1}{\eta^2} - \frac{e^{\eta}}{(e^{\eta}-1)^2} \right] \qquad (29)^*$$

$$\frac{\chi_{rt}}{\chi_o} = \frac{12}{\eta} \left[\frac{e^{\eta}}{e^{\eta}-1} - \frac{1}{\eta} \right]$$

χ_o is the value of the parallel reversible susceptibility when $\eta = 0$. Using this model $\chi_{rt} \neq \chi_{rp}$ when $\eta = 0$. Values of η, M/M_s, χ_{rp}/χ_o and χ_{rt}/χ_o are given in Table V.

Obviously χ_{rt}/χ_o is much greater using this model than using the isotropic model.

* To evaluate the integration constant note that χ_{rt} must become infinite at some value of M/M_s. It will be positive above that value and negative below. The only point where such a discontinuity can exist is for $\eta = 0$. Thus the integration constant must be zero.

TABLE V

M/M_s and χ_r/χ_o vs η for $f(\eta) = \left[\frac{1}{1-e^{-\eta}} - \frac{1}{\eta}\right]$

η	M/M_s	χ_{rp}/χ_o	χ_{rt}/χ_o
0	.500	1.000	∞
1	.582	.943	6.98
2	.656	.828	3.94
3	.720	.671	2.88
5	.806	.397	1.93
7	.857	.234	1.46
10	.900	.012	1.08
15	.933	0	.744
20	.950	0	.576
50	.980	0	.240
∞	1.000	0	0

6. COMPARISON WITH EXPERIMENT

6.1 The Parallel Case. From Figs. 12 thru 18, as described in section 4.2, one sees that for decreasing $|M|$ the experimental curves start, at high $|M|$, below the theoretical curve. The experimental curve becomes larger than the theoretical curve, passes through a maximum before $|M| = 0$ is reached, then remains less than the theoretical curve for increasing $|M|$. Fig. 19 illustrates the variation of the curves for small $|M|/M_s$ as the peak value of M reached during the cycle is altered. In Fig. 19 the ordinates have been normalized to the highest value of susceptibility measured.

These differences can be correlated with the modifications of section 5.3.1. Consider in the region of small decreasing $|M|$ a fraction D of the material to be held in metastable positions that contribute nothing to the susceptibility. The maximum value of χ will occur when the total M of the remaining material (1-D) is zero. There will still be a net magnetization in the direction of the last previous peak value contributed by D, and as seen before D is expected to increase with the magnitude of $|M|$ at that peak.

Thus the value of M/M_s for which χ is a maximum will increase with increasing peak M during the cycling. The value of χ_{max} should also decrease proportional to (1-D). This can be seen experimentally in Fig. 19. Thus Figs. 12 thru 17 should actually be normalized to the value of susceptibility occuring when the material is carefully demagnetized and H=M=0. This value can never be exceeded.

The corrections of section 5.3.2, Table IV, are small for the parallel case, so will have little effect.

The hysteresis loop of χ_{rp}/χ_o, see Fig. 18, is traced in the opposite direction when plotted against M than when plotted against H. This arises formally because H_c' as defined in section 4 is less than H_c. All measurements we have made has given H_c' of the same sign as H_c. Qualitatively, the arguments of section 5.3 for constant η instead of constant M would give the proper hysteresis loop for χ_{rp} vs. H.

This variation of χ_{rp} with M and with history is in qualitative agreement with the results of Tebble and Corner[2].

6.2 The Transverse Case. There are two opposing effects which determine the hysteresis loop for this case. Firstly, for the same reasons as the parallel susceptibility, the transverse susceptibility will go through a maximum before reaching M = 0 for decreasing $|M|$. Secondly, upon comparing the susceptibility curves for the isotropic distribution of magnetic moments and for the distribution of the model used in section 5.3.3, Table V, it is seen that the latter yields considerably higher values of χ_{rt}.

This would produce a larger χ_{rt} for increasing fields than for decreasing fields. The first effect would predominate at low fields, the second at high fields. The result is an intersection of the susceptibility curves as can

be seen on Figs. 12 thru 17 and is plotted to be especially evident in Fig. 18. The value of M/M_s at which the intersection occurs should then decrease with decreasing peak M reached during the cycle. Unfortunately we were unable to obtain experimental data for minor loops using a transverse field.

7. ACKNOWLEDGEMENTS

The authors with to thank Professor H. W. Welch, Jr. for encouraging this work; Messrs. John Newton and Ralph Olson for assistance in recording data; Professor E. Katz, Dr. L. W. Orr and Mr. M. H. Winsnes for aid during the early stages of the work.

APPENDIX

Derivation of the relationship between χ_{rp} and M. (after Brown)

A.1 General Formulation

Consider a ferromagnet to be composed of N domains per unit volume, each of fixed and equal volume. These domains are acted upon by internal forces of a reversible nature probably arising from microscopic demagnetizing factors or from walls held in potential holes with a finite radius of curvature. If these were negligible and if the entropy were negligible the system would occupy the minimum energy condition determined by the interaction of the remaining surface and volume energies. Certainly the entropy of the system is negligible. However, a pseudoentropy whose disordering arises not from thermal agitation but localized randomally oriented stresses is not negligible, as is obvious from Eqs. 10 and 11.

Brown states that the detailed mechanism of the microscopic forces are unimportant, but their energy magnitudes are important. Therefore one does not need to know the exact distribution of these localized stresses for similar results should be obtained from any of a large number of possible distributions. One such possible distribution could be gotten by considering the number of macroscopically indistinguishable ways N domains of fixed and equal volume could be microscopically arranged. This is given by:

$$W = \frac{N!}{\prod_{\gamma} (N_\gamma!)}$$

where γ is a possible direction for orientation of the domain moment. Using Stirling's approximation:

$$\ell n\, W \cong N\, \ell n\, N - \sum_{\gamma} N_{\gamma}\, \ell n\, N_{\gamma} \tag{A1}$$

The potential of the material can be written as

$$V = \sum_{\gamma} N_{\gamma} (V_{\gamma}^{V} + V_{\gamma}^{S}) \tag{A2}$$

where V_{γ}^{V} involves an energy proportional to the number of domains involved, V_{γ}^{S} depends upon the surface energy. The system is also subject to the constraint on the total number of domains:

$$N = \sum_{\gamma} N_{\gamma} \tag{A3}$$

If the system is considered to occupy a most probable position then $\ell n\, W$ should be stable with respect to variations in N_{γ}. The similarity between this distribution and that due to the conventional entropy is obvious.

V_{γ}^{V} is just the customary equation for the magnetostatic energy of a dipole in an applied field:

$$V_{\gamma}^{V} = -H_{r}\, M_{s} \cos \theta \tag{A4}$$

θ is the angle between H_{r} and the direction of orientation of the domain. The term V_{γ}^{S} involves the surface energy. This will depend upon the particular geometry involved and must be considered constant.

Taking variations of Eqs. A1, A2, A3 with respect to N_{γ} and introducing Lagrange multipliers, one obtains:

$$\left[-\ell n\, N_{\gamma} + A(V_{\gamma}^{V} + V_{\gamma}^{S}) + B\right] = 0 \tag{A5}$$

or

$$N_\gamma = \exp\left[B + a(V_\gamma^V + V_\gamma^S)\right]$$

If $n_\gamma = \frac{N_\gamma}{N}$; then:

$$n_\gamma = \frac{e^{AV_\gamma^V}}{\sum_\gamma e^{AV_\gamma^V}} = \frac{\exp\ (AH_rM_S\cos\ \theta)}{\sum_\theta \exp\ (AH_rM_S\cos\ \theta)} \tag{A6}$$

The resulting magnetization must then be given by:

$$\frac{M}{M_S} = \frac{\sum_\theta \cos\ \theta\ \exp(AH_rM_S\cos\ \theta)}{\sum_\theta \exp\ (AH_rM_S\cos\ \theta)} \tag{A7}$$

This formulation considers only magnetization by reversible processes. Therefore H_r is not the actual applied field, but is that value of field which would be necessary to bring the material to a magnetization M if no irreversible processes were involved, i.e.

$$H_r = \int_o^M \frac{dM}{\chi_r} \tag{A8}$$

A.2 Isotropic Material

For the case of isotropic material Eq. A7 becomes:

$$\frac{M}{M_S} = \frac{\frac{1}{4\pi}\ \int_o^{2\pi} d\phi\ \int_o^{\pi} \sin\ \theta d\theta\ \cos\ \theta\ e^{AH_rM_S\cos\ \theta}}{\frac{1}{4\pi}\ \int_o^{2\pi} d\phi\ \int_o^{\pi} \sin\ \theta d\theta\ e^{AH_rM_S\cos\ \theta}}$$

If $\cos\Theta = \gamma$ and $AH_rM_s = \eta$,

$$\frac{M}{M_s} = \frac{\int_{-1}^{1} d\gamma\ \gamma e^{\eta\gamma}}{\int_{-1}^{1} d\gamma\ e^{\eta\gamma}} = \frac{\frac{d}{d\eta}\left[\int_{-1}^{1} d\gamma\ e^{\eta\gamma}\right]}{\int_{-1}^{1} d\gamma\ e^{\eta\gamma}}$$

$$\int_{-1}^{1} d\gamma\ e^{\eta\gamma} = \frac{1}{\eta}\left(e^{\eta} - e^{-\eta}\right) = \frac{2}{\eta}\sinh\eta$$

Therefore:

$$\frac{M}{M_s} = \frac{\frac{1}{\eta}\cosh\eta - \frac{1}{\eta^2}\sinh\eta}{\frac{1}{\eta}\sinh\eta} = \left(\operatorname{ctnh}\eta - \frac{1}{\eta}\right) = L(\eta) \qquad \text{(A9)}$$

The parallel reversible susceptibility is given by:

$$\chi_{rp} = \frac{dM}{dH_r} = M_s \frac{d\,L(\eta)}{d\eta}\frac{\partial\eta}{\partial H_r} = AM_s^2\,L'(\eta) \qquad \text{(A10)}$$

where the prime indicates $\frac{d}{d\eta}$.

The initial susceptibility is defined by Eq. 3. Using Eq. 16 for small values of η one sees that:

$$\chi_o = \frac{AM_s^2}{3} \qquad \text{(A11)}$$

Combining Eqs. A10 and A11,

$$\frac{\chi_{rp}}{\chi_o} = 3\,L'(\eta) \qquad \text{(A12)}$$

A.3 [111] Anisotropy

Here each domain must be located in such a manner that its direction of magnetization is in the [111] direction of the crystal. If α_i is the direction cosine between M_s and the axis Ox_i, then $\alpha_i = \frac{1}{\sqrt{3}} p_i$ where $p_i = \pm 1$ for each value of i.

If ℓ_i is the direction cosine between the applied field and the crystalline axis Ox_i, then:

$$\cos \Theta = \frac{1}{\sqrt{3}} \sum_i p_i \ell_i \tag{A13}$$

After combining Eqs. A7 and A13, for a single crystal:

$$\frac{M}{M_s} = \frac{\frac{1}{\sqrt{3}} \sum_p \sum_j p_j \ell_j \exp\left[\frac{\eta}{\sqrt{3}} \sum_i p_i \ell_i \right]}{\sum_p \exp\left[\frac{\eta}{\sqrt{3}} \sum_i p_i \ell_i \right]} \tag{A14}$$

To evaluate these sums, first consider the denominator of Eq. A14. The outside sum over p is over the eight possible combinations of $(p_1, p_2, p_3) = (1,1,1)$; $(1,1,-1)$; ••••••; $(-1,-1,-1)$. Upon simplifying this is seen to be:

$$\sum_p \exp\left[\frac{\eta}{\sqrt{3}} \sum_i p_i \ell_i \right] = 8 \prod_k \cosh\left[\frac{\eta}{\sqrt{3}} \ell_k \right] \tag{A15}$$

From Eq. A15 one obtains:

$$\sqrt{3} \sum_j \ell_j \frac{\partial}{\partial(\eta \ell_j)} \left[\sum_p \exp\left(\frac{\eta}{\sqrt{3}} \sum_i p_i \ell_i\right)\right]$$

$$= \sum_p \sum_j p_j \ell_j \exp\left(\frac{\eta}{\sqrt{3}} \sum_i p_i \ell_i\right) \qquad \text{(A16)}$$

$$= 8 \sum_j \ell_j \sinh\left(\frac{\eta}{\sqrt{3}} \ell_j\right) \prod_k{}' \cosh\left(\frac{\eta}{\sqrt{3}} \ell_k\right)$$

where the prime denotes $k \neq j$. The first expression on the right side is exactly the numerator of Eq. A14. By substituting the second expression for the numerator, and Eq. A15 for the denominator in Eq. A14, one obtains:

$$\frac{M}{M_s} = \frac{1}{\sqrt{3}} \sum_j \ell_j \tanh \frac{\eta}{\sqrt{3}} \ell_j \qquad \text{(A17)}$$

for a single crystal.

To obtain the value of M/M_s for polycrystalline material it is necessary to integrate over all possible values of ℓ_j;

$$\frac{M}{M_s} = \frac{1}{\sqrt{3}} \sum_j \int \frac{d\omega}{4\pi} \ell_j \tanh \frac{\eta}{\sqrt{3}} \ell_j \qquad \text{(A18)}$$

where $d\omega$ is the differential solid angle.

Each of the three ℓ_j must be equivalent so:

$$\frac{M}{M_s} = \frac{\sqrt{3}}{4\pi} \int d\omega \, \ell \tanh \frac{\eta}{\sqrt{3}} \ell = \frac{\sqrt{3}}{4\pi} \int_0^{2\pi} d\phi \int_0^{\pi} d\theta \sin\theta \cos\theta \tanh\left(\frac{\eta}{\sqrt{3}} \cos\theta\right)$$

Let $u = \frac{\eta}{\sqrt{3}} \cos\theta$, so:

$$\frac{M}{M_s} = \frac{3\sqrt{3}}{\eta^2} \int_0^{\eta/\sqrt{3}} u \tanh u \, d u = E(\eta) \tag{A19}$$

$$\chi_{rp} = \frac{dM}{dH_r} = M_s \frac{dE(\eta)}{d\eta} \frac{\partial \eta}{\partial H} = AM_s^2 E'(\eta) \tag{A20}$$

From Eq. 17, as for the isotropic case:

$$\chi_o = \frac{AM_s^2}{3} \tag{A21}$$

Therefore, for $\left[111\right]$ anisotropy,

$$\frac{\chi_{rp}}{\chi_o} = 3E'(\eta) \tag{A22}$$

BIBLIOGRAPHY

1. Gans, R., "Equation of the Curve of Reversible Susceptibility", Physik. Z. 12, pp. 1053-1054, 1911.

2. Tebble, R. S. and Corner, W. D., "Investigation on the Reversible Susceptibility of Ferromagnetics", Proc. Phys. Soc. 63, pp. 1005-1016, 1950.

3. Rado, G.E.; Wright, R.W. and Emerson, W.H., "Ferromagnetism at Very High Frequencies. III. Two Mechanisms of Dispersion in a Ferrite", Phys. Rev. 80, pp. 273-280, 1950.

   Rado, G.E.; Wright, R.W.; Emerson, W.H. and Terris, A., "IV. Temperature Dependence of the Magnetic Spectrum of a Ferrite", Phys. Rev. 88, pp. 909-915, 1952.

4. Becker, R. and Doring, W., "Ferromagnetisms", Edward Bros. Ann Arbor, pp. 154, 1943.

5. Kersten, M., "The Effect of Elastic Tension on the Magnitude of the Initial Permeability", Z. Tech. Physik 12, pp. 665-669, 1931.

6. Brown, W.F., Jr., "Domain Theory of Ferromagnetics under Stress", Phys. Rev. 52, pp. 325-334, 1937.

   "II. Magnetostriction of Polycrystalline Material", Phys. Rev. 53, pp. 482-491, 1938.

   "III. The Reversible Susceptibility", Phys. Rev. 54, pp. 279-287, 1938.

7. Brown, W.F., Jr., "Theory of Reversible Magnetization in Ferromagnetics", Phys. Rev. 55, pp. 568-578, 1939.

8. Brown, W.F., Jr., Private correspondence

DISTRIBUTION LIST

1 Copy	Director, Electronic Research Laboratory Stanford University Stanford, California Attn: Dean Fred Terman
1 Copy	Commanding Officer Signal Corps Electronic Warfare Center Fort Monmouth, New Jersey
1 Copy	Chief, Engineering and Technical Division Department of the Army Washington 25, D. C. Attn: SIGJM
1 Copy	Chief, Plans and Operations Division Office of the Chief Signal Officer Washington 25, D. C. Attn: SIGOP-5
1 Copy	Countermeasures Laboratory Gilfillan Brothers, Inc. 1815 Venice Blvd. Los Angeles 6, California
1 Copy	Commanding Officer White Sands Signal Corps Agency White Sands Proving Ground Las Cruces, New Mexico Attn: SIGWS-CM
1 Copy	Commanding Officer Signal Corps Electronic Research Unit 9560th SU Mountain View, California
1 Copy	Mr. Peter H. Haas High Frequency Standard Section Central Radio Propagation Laboratory National Bureau of Standards Washington 25, D. C.
1 Copy	Dr. J. K. Galt Bell Telephone Laboratories, Inc. Murray Hill, New Jersey

1 Copy	Dr. R. M. Bozorth Bell Telephone Laboratories, Inc. Murray Hill, New Jersey
1 Copy	Dr. G. T. Rado Naval Research Laboratory Washington 25, D. C.
75 Copies	Transportation Officer, SCEL Evans Signal Laboratory Building No. 42 Belmar, New Jersey FOR - Signal Property Officer Inspect at Destination File No. 25052-PH-51-91(1443)
1 Copy	H. W. Welch, Jr. Engineering Research Institute University of Michigan Ann Arbor, Michigan
1 Copy	Document Room Willow Run Research Center University of Michigan Willow Run, Michigan
11 Copies	Electronic Defense Group Project File University of Michigan Ann Arbor, Michigan
1 Copy	Engineering Research Institute Project File University of Michigan Ann Arbor, Michigan